Link ER ion homeostasis maintained by an ER anion channel to ALS

Yichang Jia (yichangjia@mail.tsinghua.edu.cn)
Tsinghua University

Liang Guo
Tsinghua-Peking Joint Center for Life Sciences, Tsinghua University, Beijing, 100084, China.

Qionglei Mao
Shanghai Institute of Materia Medica, Chinese Academy of Sciences.

Ji He
Peking University Third Hospital

Xiaoling LIU
School of Pharmaceutical Sciences,Tsinghua University

Xuejiao Piao
Tsinghua University

Li Luo
Tsinghua University

Xiaoxu Hao
Zhejiang University

Bailong Xiao
State Key Laboratory of Membrane Biology, Tsinghua-Peking Joint Center for Life Sciences, Beijing Advanced Innovation Center for Structural Biology, IDG/McGovern Institute for Brain Research, School
https://orcid.org/0000-0002-2386-3322

Dongsheng Fan
Department of Neurology, Peking University Third hospital

Zhaobing Gao
Shanghai Institute of Materia Medica, Chinese Academy of Sciences

Biological Sciences - Article

Keywords: Anion channel, endoplasmic reticulum (ER), ion homeostasis, ER stress, ALS.

Posted Date: May 27th, 2021

DOI: https://doi.org/10.21203/rs.3.rs-536643/v1

Title： Link ER ion homeostasis maintained by an ER anion channel to ALS

Authors/Affiliations：

Liang Guo[1,3,4,5*], Qionglei Mao[2,6*], Ji He[7*], Xiaoling Liu[5,8], Xuejiao Piao[1,3,4,5], Li Luo[4,9], Xiaoxu Hao[2,10,11], Bailong Xiao[1,5,8], Dongsheng Fan[7,12#], Zhaobing Gao[2,6#], and Yichang Jia[1,4,5,9#]

[1]Tsinghua-Peking Joint Center for Life Sciences, Tsinghua University, Beijing, 100084, China.
[2]CAS Key Laboratory of Receptor Research, State Key Laboratory of Drug Research, Shanghai Institute of Materia and Medica, Chinese Academy of Sciences, 555 Zuchongzhi Road, Shanghai, 201203, China.
[3]School of Life Sciences, Tsinghua University, Beijing, 100084, China.
[4]School of Medicine, Tsinghua University, Beijing, 100084, China.
[5]IDG/McGovern Institute for Brain Research, Tsinghua University, Beijing, 100084, China.
[6]University of Chinese Academy of Sciences, No.19 (A) Yuquan Road, Beijing, 100049, China
[7]Department of Neurology, Peking University Third Hospital, Beijing, 100191, China.
[8]School of Pharmaceutical Sciences, Tsinghua University, Beijing, 100084, China.
[9]Tsinghua Laboratory of Brain and Intelligence, Beijing, 100084, China
[10]School of Pharmaceutical Sciences, Zhejiang University, Hangzhou, 310058, China.
[11]School of Medicine, Zhejiang University City College, Hangzhou, 310015, China.
[12]Beijing Municipal Key Laboratory of Biomarker and Translational Research in Neurodegenerative Diseases, Beijing, 100191, China
*These authors contributed equally to this work.

Corresponding authors
Please address correspondence to: Dongsheng Fan, MD, PhD
Neurological Department of Peking University Third Hospital, Haidian District, Beijing No. 49, North Garden Road, Haidian District, Beijing, 100191, China.
Tel: 86-10-82265032, Email: dsfan2010@aliyun.com

Corresponding authors
Please address correspondence to: Zhaobing Gao, Ph. D.
CAS Key Laboratory of Receptor Research, State Key Laboratory of Drug Research, Shanghai Institute of Materia Medica, Chinese Academy of Sciences, 555 Zuchongzhi Road, Shanghai, 201203, China.
Tel: 86-21-20239067, Email: zbgao@simm.ac.cn

Corresponding author
Please address correspondence to: Yichang Jia, Ph. D.
School of Medicine, Medical Science Building, Room D204, Tsinghua University, Beijing, 100084, P. R. China
Tel: 86-10-62781045, Email: yichangjia@tsinghua.edu.cn

Abstract: (200 words)

Although anion channel activities have been demonstrated in sarcoplasmic reticulum/endoplasmic reticulum (SR/ER), their molecular identities and functions remain unclear. Here, we link rare variants of *CLCC1* (Chloride Channel CLIC Like 1) to ALS (amyotrophic lateral sclerosis). We demonstrate that CLCC1 is a pore-forming component of an ER anion channel and that ALS-associated mutations impair the channel activity. CLCC1 unitary conductance is inhibited by luminal Ca^{2+} but facilitated by phosphatidylinositol 4,5-bisphosphate (PIP2). We identified a conserved lysine 298 (K298) in CLCC1 intraluminal loop as the critical PIP2-sensing residue. CLCC1 maintains steady-state $[Cl^-]_{ER}$ and morphology and regulates ER Ca^{2+} homeostasis including steady-state $[Ca^{2+}]_{ER}$ and efficiency of internal Ca^{2+} release. ALS-associated mutant CLCC1 increase steady-state $[Cl^-]_{ER}$ and impair ER Ca^{2+} homeostasis. Phenotypic comparisons of multiple *Clcc1* mutant alleles, including ALS-associated mutations, reveal a CLCC1 dosage-dependence in severity of disease phenotypes *in vivo*. Conditional knockout of *Clcc1* cell-autonomously causes motor neuron loss and ER stress, misfolded protein accumulation, and characteristic ALS pathologies in the spinal cord. Thus, we argue that disruption of ER ion homeostasis maintained by CLCC1 underlies etiology of neurodegenerative diseases.

Keywords:

Anion channel, endoplasmic reticulum (ER), ion homeostasis, ER stress, ALS.

Although Cl^- is the most abundant anion in living cells, chloride currents and their functional significance had been understudied until the CLC family of chloride channels and CFTR (cystic fibrosis transmembrane conductance regulator) were cloned and their dysfunctions were linked to human diseases [1-4]. In addition to those on the cell surface, Cl^- channels have long been proposed to exist in the intracellular membrane-bound organelles [3,5]. However, the previously postulated intracellular Cl^- channels, like CLCAs (chloride channel Ca^{2+}-activated) and CLICs (chloride intracellular channels), are now considered not likely to function as anion channels [6,7]. Therefore, the molecular identities and functions of organellar anion channels, including those in the SR/ER, remain largely unknown.

As the major internal Ca^{2+} store, Ca^{2+} release from SR/ER is mediated mainly by two cation channels, RyRs (ryanodine receptors) and IP3Rs (inositol 1,4,5-trisphosphate receptors) [8-10]. Other cation channels in SR/ER membranes regulate the Ca^{2+} release/content through different mechanisms [11]. For example, TRICs (TRimeric Intracellular Cation channels) are potassium channels that regulate Ca^{2+} release via a counter-ion mechanism, in which the influx of K^+ through TRICs balances the loss of positive charges from the SR/ER as a result of the Ca^{2+} efflux, which helps maintain the driving force for continued Ca^{2+} release [12]. In addition to cations, anions have also been proposed to regulate ER Ca^{2+} release through the counter-ion mechanism, and various Cl^- channel activities

have been long demonstrated in microsome preparations [11,13-17]. A previous study using mouse forward genetics revealed that loss of CLCC1 (Chloride Channel CLIC Like 1), an ER resident protein, leads to ER stress and neurodegeneration [18]. However, despite the name, CLCC1 has little sequence similarity with CLIC family members or any known ion channels. In addition, question remains whether the recorded chloride currents in microsome prepared from the CLCC1 overexpressing cells were actually mediated by CLCC1 [19]. Therefore, further evidence is needed to know if CLCC1 functions as an anion channel.

ER stress and its related misfolded protein accumulation are one of the central pathogenic pathways underlying neurodegenerative diseases, including ALS [20-22]. Here, we link *CLCC1* rare mutations to ALS and demonstrate CLCC1 is the pore-forming component of an ER anion channel. Dysfunction of CLCC1 impairs steady state ER [Cl^-] and misregulates ER Ca^{2+} homeostasis and leads to ER swelling, ER stress, and protein misfolding. Therefore, we argue that misregulation of ER ion homeostasis maintained by CLCC1 underlies etiology of neurodegenerative diseases.

Rare genetic variances in *CLCC1* found in a Chinese ALS cohort

To identify novel rare mutations potentially associated with ALS, we performed whole exome sequencing in a Chinese cohort (670 sporadic ALS patients and 1910 controls). We identified 9 rare variances in *CLCC1* in the patients, including 7 nonsynonymous and 2 stopgain mutations (Fig. 1a, Extended Data Fig. 1, and Supplementary Table 1). Among the mutations (Fig. 1b), the S263R and W267R mutations have not been found in the public databases nor in our controls (Supplementary Table 1). No mutations in known ALS-causing genes were detected in the patients carrying S263R or W267R mutation. Notably, two geographically and genetically unrelated patients with similar clinical phenotypes shared the same S263R mutation (Supplementary Table 1). The two mutations change Ser and Try to Arg, suggesting that they perturb local steric hindrance and surface potential. CLCC1 is ubiquitously expressed and its disruption has been shown to lead to ER stress and neurodegeneration in mice [18]. A burden analysis [23] was further carried out and revealed that *CLCC1* is associated with ALS (p = 1.51×10^{-6}, with OR = 5.72), reaching suggestive significance (Fig. 1c).

ALS mutations S263R and W267R reduce CLCC1 expression and promote ER stress and protein misfolding *in vivo*

Homozygous knockout of *Clcc1* in mice is lethal, indicating *Clcc1* is essential (Extended Data Fig. 2a and Supplementary Table 2). Evolutionarily, CLCC1

orthologues appear in vertebrate bot not invertebrate (Fig. 1d). Human and mouse CLCC1 share 73% identity, but S263 and W267 are conserved between the two species. To examine the biological consequence of S263R and W267R *in vivo*, we generated S263R and W267R knock-in mouse lines (Extended Data Fig. 2b and 2c). Mice heterozygous for S263R and W267R were viable and fertile, and no obvious ER stress and protein misfolding was disclosed in S263R heterozygous mutant (S263R/+) cerebella (Fig. 1e). However, Bip upregulation and ubiquitin-positive misfolded protein accumulation were documented in the cerebella of mice compound heterozygous for S263R and the *NM2453* allele (S263R/*NM*) – where an IAP (intracisternal A-particle) insertion in the intron 2 of *Clcc1* greatly reduces the expression of CLCC1 protein to ~10% of that in wildtype animals [18]. Like S263R/*NM* mutants, the W267R/*NM* mutants displayed the similar extent of ER stress and protein misfolding in cerebella (Fig. 1e). In contrast, mice heterozygous for *NM2453* allele (*NM*/+) were normal without ER stress in cerebella [18]. In addition to the pathologies, both S263R and W267R mutations reduced mutant CLCC1 expression to a similar extent, suggesting that severity of mutant *Clcc1* phenotypes depends on the dosage of CLCC1 protein (Fig. 1f). Indeed, we failed to harvest W267R/KO pup, suggesting that the ALS-associated mutant alleles are functionally damaging *in vivo*, which is independent of *NM2453* allele (Supplementary Table 2). Therefore, our data support the

notion that ALS-associated S263R and W267R mutations are potential disease-causing.

CLCC1 forms homomultimer in the ER membrane

Based on its primary sequence, CLCC1 shares little sequence similarity with any known ion channel and is predicted to contain three transmembrane segments (TMs) and an N-terminal signal peptide (Fig. 2a). We generated antibodies against the N- and C-termini of CLCC1 (Extended Data Fig. 3a). Using the C-terminal antibody, we confirm that as suggested by a previous report [18] CLCC1 is predominantly ER-localized, as demonstrated by its co-localization with CALNEXIN, an ER resident protein (Extended Data Fig. 3b).

To understand how CLCC1 functions in the ER, we treated human 293FT cells with disuccinimidyl suberate (DSS), a crosslinker with a spacer length of 11.4 Å. The C-terminal antibody detected high molecular weight complexes in a DSS dosage-dependent manner from whole cell lysate. From the complex sizes, we speculated that CLCC1 forms homomultimers (Fig. 2b), which was supported by co-immunoprecipitations of differentially tagged CLCC1 co-expressed in the same cells (Extended Data Fig. 4a) and of exogenous tagged CLCC1 with endogenous CLCC1 (Extended Data Fig. 4b). In addition, purified CLCC1 N- and C-terminal polypeptides formed homomultimers *in vitro* in a DSS-dependent manner (Extended Data Fig. 4c and 4d), and disulfide bonds between cysteine residues

are not necessary for the multimerization, as shown electrophoresis of cysteine-less mutant polypeptides (Extended Data Fig. 4e and 4f). For the purified C-terminal polypeptide, homomultimers were detected in denaturing gels after crosslinking with formaldehyde, suggesting a close distance of 2-3 Å [24] between monomers (Extended Data Fig. 4g). Consistent with our cell culture data (Fig. 2b), the purified full-length mouse CLCC1 (mCLCC1) gave a major high molecular weight peak by chromatographic column separation (Fig. 2c), indicating that the full-length CLCC1 also forms homomultimers *in vitro*. Taken together, our data suggest that CLCC1 forms homomultimer in the ER membrane.

CLCC1 is a pore-forming component of an anion channel and ALS-associated mutations impair the channel activity

Incorporation of the purified full-length mCLCC1 (Fig. 2c) into planar lipid bilayer resulted in frequent inward currents at 0 mV (-2.2 ± 0.1 pA) in asymmetric KCl solutions (In/Ex, 150/15 mM) and the currents became outward at 90 mV (1.6 ± 0.1 pA) (Fig. 2d). As a negative control, the protein purification buffer without protein gave rise to no current (Fig. 2d). Based on the fit of the current-voltage relationship, the reversal potentials were determined to be 56.8 mV (In/Ex, 150/15 mM KCl) and -60.3 mV (In/Ex, 15/150 mM KCl), which are close to the calculated values for Cl^- by Nernst equation, and the slope conductance was 39.9 ± 1.0 pS (mean ± SEM). The permeability ratio of $P(Cl^-)$ to $P(K^+)$ is about 100 to 1 and

similar results were obtained by using asymmetric NaCl solutions (Fig. 2d). Consistent with the single channel results, the reversal potential obtained from studying macroscopic currents was 61.9 mV in 15/150 mM KCl (In/Ex) (Extended Data Fig. 5), further supporting the anion selectivity.

Next, we examined CLCC1 channel permeability to various anions, including Br^-, SO_4^{2-}, and NO_3^-, by adding 150 mM KCl in *cis* (In) and equal electric charges of KBr, K_2SO_4, or KNO_3 in the *trans* (Ex) chamber (Fig. 2e). The relative permeabilities of these anions to Cl^- were 16.51 (P_{Br}/P_{Cl}), 1.55 (P_{SO4}/P_{Cl}), and 0.22 (P_{NO3}/P_{Cl}), respectively, indicating a sequence of the CLCC1 anion selectivity of $P_{Br} > P_{SO4} > P_{Cl} > P_{NO3}$. In these experiments, no cation permeation was detected.

To examine how S263R and W267R alter CLCC1 channel activity, we incorporated the purified human wildtype (hWT), S263R or W267R mutant CLCC1 proteins into the lipid bilayer for single channel analysis. The slope conductances of both S263R and W267R were significantly lower than that of hWT (Fig. 2f). Collectively, our results demonstrate that CLCC1 is a pore-forming component of an anion channel and that ALS-associated mutations impair CLCC1 unitary conductance.

ER membrane topology of CLCC1 and its inhibition by luminal calcium

To examine CLCC1 topology in the ER membrane, we treated microsomes prepared from wildtype mouse cerebella and livers [25] with trypsin and analyzed the

remaining CLCC1 fragments with our N- and C-terminal antibodies (Extended Data Fig. 3a). In the absence of Triton X-100, the N-terminus and the first and second loops of CLCC1 and an ER lumen resident protein Bip were protected from trypsinization, but the C-terminus of CLCC1 was not (Fig. 2g and Extended Data Fig. 3c). As expected for membrane enclosure, the protection was disrupted by Triton X-100, suggesting that CLCC1 N-terminus and the second loop reside in ER lumen while C-terminus faces cytoplasm.

Interestingly, when we applied MTSET (methanethiosulfonate-ethyltrimethylammonium) [26], a membrane-impermeant thiol reagent that modifies cysteine residues, in *trans* but not to the *cis* side of the chamber we applied the purified CLCC1, the CLCC1 currents were suppressed (Fig. 2h), suggesting that a specific orientation of CLCC1 in the bilayer is responsible for the current. Based on the topology (Fig. 2g), cysteine residues are located in both the cytoplasm and ER lumen sides of CLCC1 and C350 lies at the end of TM3 (Fig. 2i). Protein alignment among different species revealed that C350 is in a consecutive row of four residues (FCYG), although it is less conserved than the other three surrounding resides (Fig. 2j). Instead of FCYG in *Homo sapiens* and *Mus musculus*, FFYG appears in *Xenopus tropicalis*, which prompted us to mutate C350 to F. C350F mCLCC1 is expressed and its chromatographic behavior is similar to wildtype mCLCC1 (Extended Data Fig. 6a). Importantly, C350F

restored the CLCC1 currents even when MTSET was applied in *trans* side (Fig. 2h), suggesting that MTSET acts on C350 to modify the channel activity and the *trans* side is the CLCC1 cytoplasm side in the reconstructed lipid bilayer. Application of DIDS (4,4'-Diisothiocyano-2,2'-stilbenedisulfonic acid), a chloride transporter/channel blocker [4,27], significantly inhibited CLCC1 channel activity (Extended Data Fig. 6b and 6c). Consistent with MTSET acting on C350, C350F largely restores the DIDS inhibition on channel open probability (P_o), suggesting that C350 is close to the CLCC1 conduction pathway.

Because ER luminal Ca^{2+} is much higher than cytoplasm, we then asked whether Ca^{2+} is able to differentially regulate CLCC1 channel activity from ER luminal or cytoplasmic side. Application of Ca^{2+} in *cis*/ER lumen side blocked the CLCC1 channel activity, which could be partially rescued by addition of equal molar EGTA, a Ca^{2+} chelating agent (Fig. 2k and 2l). However, the same application in *trans*/cytoplasm side had no effect on the channel activity. Therefore, we conclude that, at least in our reconstructed lipid bilayer setting, high concentration of Ca^{2+} at the ER lumen side inhibits CLCC1 channel activity.

CLCC1 maintains steady state $[Cl^-]_{ER}$ and ER morphology

To examine whether CLCC1 is involved in regulation of $[Cl^-]_{ER}$, we employed a previously optimized YFP Cl^- sensor that responds to Cl^- concentration change with super sensitivity and photostability [28]. To create a ratiometric ER Cl^- sensor, we built a signal sequence, a DsRed internal control, and an ER retention motif

into the Cl^- sensor, which we named RaMoride^{ER} (Fig. 3a). ER localization of RaMoride^{ER} was confirmed by its colocalization with ER resident protein CALNEXIN (Fig. 3b). The ratio between YFP to Ds-Red signals responded correspondingly when extracellular [Cl^-] ([Cl^-]$_{Extra}$) was switched from 140mM to 100 or 0 mM (Extended Data Fig. 7a and 7b).

To examine ALS-associated rare variants on [Cl^-]$_{ER}$, we expressed hWT, M29T, S263R, or W267R mutant CLCC1 in 293FT cells stably expressing RaMoride^{ER} together with an engineered near-infrared fluorescent protein, miRFP670S [29], which allowed us to sort the CLCC1 expressing cells but not disturbing the RaMoride^{ER} signals (Fig. 3a and 3c). Compared to hWT, S263R or W267R but not M29T mutant CLCC1 significantly increased steady state [Cl^-]$_{ER}$, supporting that S263R and W267R are functionally damaging mutations (Fig. 3c and 3d). Consistent with the essential role of CLCC1 *in vivo*, we failed to generate a *CLCC1* KO 293FT cell line by Crispr/Cas9. Instead, we knocked down *CLCC1* with two individual shRNAs (H3 and H4) (Fig. 3e). Although the two shRNAs had different *CLCC1* knockdown efficiencies (for H3, 22.5$\pm$0.6% of scrambled control; for H4, 45.25$\pm$2.1% of scrambled control), both of them significantly increased steady state [Cl^-]$_{ER}$ to a similar extent in comparison with scrambled shRNA control (Fig. 3f).

The concentration of electrically charged osmolytes, such as Cl^-, inside a cell or intracellular membrane-bound organelle governs the volume of the

compartment [5,30]. Therefore, we asked whether depletion of *CLCC1* changes ER volume. To this end, we collected 293FT cells expressing scrambled control or *CLCC1* shRNAs and applied for transmission electron microscopy (TEM) (Fig. 3g and 3h). Enlarged and stubby ER morphology was documented in cells expressing the individual *CLCC1* shRNA. In contrast, ribosome-bound and tubule-like ER was shown in the scrambled controls. In order to quantitatively reflect ER morphology, we measured ER width in these three groups of cells. ER width in the two individual *CLCC1* shRNA groups was significantly increased as compared to scrambled shRNA control. ER width in H3 shRNA group, where there is higher knockdown efficiency, was significantly larger than that in H4 shRNA group, suggesting a *CLCC1* dosage-dependence in the effect on ER swelling.

CLCC1 facilitates internal Ca^{2+} release and ALS-associated mutations impair the Ca^{2+} release

ER-localized ion channels have been proposed to control ER Ca^{2+} mobilization through a counter-ion mechanism [11,14,16,17]. We then asked whether as an ER chloride channel CLCC1 is involved in regulation of ER Ca^{2+} release. Knockdown of *CLCC1* by two individual shRNAs markedly reduced internal Ca^{2+} release induced by ATP (Fig. 4a), which triggers ER Ca^{2+} release by generating IP3 that activates IP3Rs [10]. Compared to mock control and scrambled shRNA,

knockdown of *CLCC1* by two individual shRNA not only significantly reduced the amplitude, but also the rate (as reflected by the increase in time-to-peak), of ATP-induced Ca^{2+} release (Fig. 4b and 4c). Although the two shRNAs had different *CLCC1* knockdown efficiencies, they impaired the ATP-induced Ca^{2+} amplitude and rate to a similar extent.

Analysis of the Ca^{2+} release dynamics in individual cells revealed that *CLCC1* knockdown impaired ATP-induced Ca^{2+} oscillation (Extended Data Fig. 8a and 8b). Whereas less than 10% of cells exhibited only one ATP-induced Ca^{2+} spike in mock control or scrambled shRNA groups, the proportion was more than a half in the *CLCC1* knockdown group. The impairment of ATP-induced Ca^{2+} release seems not to be caused by shRNA off-target effects, because the reexpression of full-length (WT) mCLCC1 restored the release damaged by H3 shRNA alone (Fig. 4d and 4e). In contrast, expression of mutant mCLCC1 lacking the ER lumen resident 2^{nd} loop ($\Delta 2^{nd}$ loop) did not, suggesting the 2^{nd} loop of CLCC1 is crucial for its functions. Interestingly, both ALS-associated S263R and W267R mutations located in the 2^{nd} loop also significantly affected the internal Ca^{2+} release relative to wildtype hCLCC1 (hWT) (Fig. 4f), further confirming the damaging effect of the mutations on channel function.

Next, we asked whether CLCC1 regulates internal Ca^{2+} release through RyRs (ryanodine receptors), the predominant intracellular Ca^{2+} channels expressed in

cardiomyocytes [10] . To this end, we stimulated cardiomyocytes cultured from wildtype (+/+) and *NM2453* mutant (*NM*/*NM*) mice with caffeine, an agonist for RyR-mediated Ca^{2+} release. RyR-mediated Ca^{2+} release was significantly reduced in *NM*/*NM* cardiomyocytes as compared to +/+ controls (Extended Data Fig. 8c), demonstrating that CLCC1 facilitates ER Ca^{2+} efflux through regulation of the release process *per se* rather than regulation of a particular type of Ca^{2+} release channels.

CLCC1 dosage is crucial for maintenance of steady state $[Ca^{2+}]_{ER}$ level

To examine whether the impaired Ca^{2+} release upon *CLCC1* knockdown results from a reduction in ER Ca^{2+} load, we depleted the ER Ca^{2+} store with cyclopiazonic acid (CPA), an inhibitor of sarco/endoplasmic reticulum Ca^{2+}-ATPase (SERCA) [31]. Knockdown of *CLCC1* by H3 but not H4 shRNA significantly reduced CPA-sensitive cytosolic Ca^{2+} rise (Fig. 4g-4i), suggesting that impairment of ER Ca^{2+} content depends on CLCC1 dosage as H3 has higher knockdown efficiency than H4 shRNA (Fig. 3e).

Given that depletion of *CLCC1* increases ER volume (Fig. 3g and 3h), we next asked whether $[Ca^{2+}]_{ER}$ is also impaired. We employed a previously reported low affinity Ca^{2+} probe, ER-GCaMP6-210 [32], which correctly responded to CPA-induced internal Ca^{2+} depletion and follow-up ionomycin-mediated extracellular Ca^{2+} replenish (Extended Data Fig. 9). Compared to mock and scrambled

322 shRNA controls, knockdown of *CLCC1* by both H3 and H4 shRNAs significantly
323 decreased steady state $[Ca^{2+}]_{ER}$ level in cells expressing ER-GCaMP6-210 (Fig. 4j
324 and 4k). The impairment caused by H3 shRNA was more severe than that by H4
325 shRNA, suggesting that depletion of *CLCC1* decreases steady state $[Ca^{2+}]_{ER}$ level
326 in a dosage-dependent manner.

327 **A conserved lysine (K298) is responsible for PIP2 facilitation of CLCC1**
328 **channel activity**

329 As a necessary cofactor of many ion channels, PIP2, an acidic phospholipid of the
330 cell membrane, has been implicated in the regulation of ion channel functions,
331 including of intercellular cation channels [33-35]. To examine whether PIP2 affects
332 CLCC1 channel activity, we included 2% PIP2 in the planar phospholipid bilayer.
333 Interestingly, PIP2 significantly increased the slope conductance (80.1 ± 2.5 pS)
334 and the open probability (P_o) of wildtype mCLCC1 (Fig. 5a and 5b). Given that
335 PIP2 regulates ion channels by binding to certain positively charged residues in
336 the channel protein [34,35], we looked for positively charged residue(s) in CLCC1 and
337 a positively charged lysine (K298) drew our attention (Fig. 5c). It lies in a
338 consecutive row of six conserved residues-VPPTKA in the 2nd loop, which is
339 required for CLCC1 facilitation of internal Ca^{2+} release (Fig. 4d and 4e). In
340 addition, K298 is downstream of two proline residues, which usually present strong
341 conformational rigidity, and lies at the beginning of a predicted alpha-helix.

We expressed and purified K298A mutant mCLCC1 and incorporated it into the lipid bilayer in the absence of PIP2, the mutant protein exhibited single channel activity with a slope conductance of 31.8 ± 0.7 pS, slightly lower than that of wildtype mCLCC1 (39.9 ± 1.0 pS) (Fig. 5a, 5d, and 5f). The P_o at 0 mV did not differ from that of wildtype mCLCC1 (Fig. 5a and 5f). Next, we mutated K298 to the negatively charged residue glutamate (K298E). Like K298A, K298E also has little effect on the channel activity in absence of PIP2 (Fig. 5f). However, unlike wildtype mCLCC1 responsible to PIP2 (Fig. 5b and 5e), both K298A and K298E mutants abolished the responses, in terms of conductance and P_o (Fig. 5e and 5f). Therefore, we conclude that PIP2 facilitates CLCC1 channel activity and a conserved K298 in the 2nd loop is responsible for the facilitation.

In comparison to the K298A mutant protein in the lipid bilayer assay, proteins with the ALS patient mutations showed slope conductance that were significantly lower than that of hWT in presence of PIP2 (Extended Data Fig. 10a-10c). However, P_o of S263R and W267R did not differ from that of hWT in absence and presence of PIP2, respectively (Extended Data Fig. 10d). Like hWT, S263R and W267R mutant CLCC1 were in response to PIP2 (Extended Data Fig. 10c). Therefore, we conclude that S263R and W267R located in the 2nd loop and close to K298 impair CLCC1 channel activity not through disruption of the PIP2-mediated facilitation.

K298 is crucial for CLCC1 regulation of internal Ca^{2+} release

If K298 is functionally important for CLCC1 channel activity, we wondered whether K298 is equally important for internal Ca^{2+} release. To examine this, we employed a lentiviral inducible system to stably express wildtype and K298A mutant mCLCC1 in 293FT cells in a controllable manner (Extended Data Fig. 11a). Expression of exogenous mCLCC1 proteins was induced after application of doxycycline (Dox) (Extended Data Fig. 11b). Both the exogenous wildtype and K298A mutant mCLCC1 interacted with the endogenous hCLCC1 (Extended Data Fig. 11c), as shown by co-immunoprecipitation, supporting complex formation by exogenous mCLCC1 and endogenous hCLCC1 (Extended Data Fig. 4b). Induction of wildtype mCLCC1 did not alter the amplitude and rate of ATP-induced Ca^{2+} release (Fig. 5g-5i). However, expression of K298A mutant mCLCC1 significantly suppressed such activities, as shown by the reduction in both the amplitude and rate when compared to un-induced (minus Dox) cells or cells induced to express wildtype mCLCC1. In addition, induction of K298A mutant mCLCC1 expression, but not wildtype mCLCC1, decreased the number of ATP-induced Ca^{2+} oscillation (Extended Data Fig. 11d and 11e). These findings are all similar to that found in *CLCC1*-knockdown cells (Fig. 4a-4c and Extended Data Fig. 8a and 8b), suggesting a dominant-negative effect of the mutant protein in CLCC1 channel function. Taken together, our findings reveal that a conserved

K298 in the 2nd loop is functionally important for CLCC1 to regulate the internal Ca^{2+} release.

K298A mutation promotes motor neuron loss and enlarges ER volume *in vivo*

To examine the *in vivo* effect of mutating the conserved K298 residue, as it is critical for PIP2 facilitation on CLCC1 channel activity and internal Ca^{2+} release, we generated K298A knock-in mouse (Extended Data Fig. 12a and 12b). Although expression of K298A mutant mRNA and protein was confirmed by Sanger sequencing and mass spectrometry (Extended Data Fig. 12c-12e), the expression level of K298A mutant protein was as low as that of the *NM2453* allele (Fig. 5j), reminiscent of ALS-associated S263R and W267R mutant CLCC1 (Fig. 1f). Like *Clcc1* KO (Supplementary Table 2), we failed to produce mouse homozygous for K298A (Supplementary Table 3), indicating that K298 is a key residue for CLCC1 expression and its essential function *in vivo*.

Compound heterozygotes with the *NM2453* and K298A mutations (*NM*/K298A) were viable but displayed severe body weight loss, hind leg weakness, trunk shaking, tail flagging, abnormal gaits, and ataxia phenotypes as early as 3 months of age (Supplementary Movie 1), much earlier than the phenotype onset shown in the *NM*/*NM* mice (> 12 month of age) [18]. Like *NM*/*NM* mice, the compound heterozygotes displayed ER stress (Fig. 5k) and neuron degeneration in cerebellar

granule neurons (Extended Data Fig. 12f). ER stress was also evidenced in hippocampal granule neurons in the compound heterozygotes but not in *NM*/*NM* mice (Extended Data Fig. 12g). As rare *CLCC1* mutations were found in ALS (Fig. 1) and the severe motor impairment and hind leg muscle weakness were shown in *NM*/K298A mice (Supplementary Movie 1), we next examined motor neuron pathologies in these compound heterozygotes mice. Indeed, ubiquitin-positive inclusions in ChAT-positive motor neurons and their number loss, two key ALS pathologies, were evidenced in the mutant spinal cords (Fig. 5l and 5m), supporting *CLCC1* is a potential ALS-causing gene.

As knockdown of *CLCC1* impairs ER ion homeostasis and leads to ER swelling (Fig. 3), we next asked whether dysfunction of CLCC1 impairs ER morphology *in vivo*. To this end, we examined the cerebella from wildtype and K298A/*NM* mice by TEM. We observed that instead of ribosome-bound and tubule-like ER morphologies observed in wildtype cerebellar granule neurons, the mutant neurons harbored enlarged, stubby, and less ribosome-bound ER (Fig. 5n). Indeed, the ER width of mutant granule neurons was significantly increased compared to that of wildtype (Fig. 5o). Taken together, our findings demonstrate that disruption of channel function by the K298A promotes ER stress and motor neuron loss and enlarges ER volume in the diseased neuron *in vivo*.

Increased penetrance of K298A allele and cell-autonomous effect of CLCC1 loss in motor neuron loss

In the K298A/+ colony, we were surprised to find that a few (12/182, K298A/+*) animals appeared to exhibit severe phenotypes as early as postnatal 90.9 ± 5.5 days (Fig. 6a-6c and Supplementary Movie 2), reminiscent of the phenotypes shown in *NM*/K298A (Fig. 5 and Supplementary Movie 1). Because dosage of CLCC1 is critical for the mutant phenotypes, we examined CLCC1 expression in various tissues in these K298/+* animals. As expected, CLCC1 expression level was significantly decreased in these tissues compared to that of wildtype and K298A/+ animals (Fig. 6d and Extended Data Fig. 13a). The decreased CLCC1 expression seems not to be explained by the decreased *Clcc1* mRNA (Extended Data Fig. 13b). Because ALS-associated mutations we identified appear dominant, increased disease penetrance of K298A heterozygous mutant CLCC1 weights the physiological relevance to ALS.

To gain insight into cell-autonomous or non-cell-autonomous effect of *Clcc1* loss-of-function in motor neuron degeneration, we generated *Clcc1* floxed (fl) mouse (Fig. 6e) and crossed it to *ChAT-Cre* mouse [36], to knockout *Clcc1* in ChAT-positive motor neuron in spinal cord. ER stress was evidenced by upregulation of both Bip and ERp72 in ChAT-positive motor neurons in *ChAT-Cre*/+;*fl*/*fl* but not *ChAT-Cre*/+;*fl*/+ spinal cords (Fig. 6f and 6g). Misfolded protein accumulation

was also evidenced by upregulation of ubiquitin in these *Clcc1* conditional KO neurons (Fig. 6f and 6g). Compared to nucleus-localized TDP-43 in *ChAT-Cre*/+;*fl*/+ motor neurons, cytoplasm-mislocalized and ubiquitin-positive TDP-43 (Fig. 6h), one of the pathological hallmarks of ALS [37-39], were documented in the conditional KO neurons. Indeed, all the *ChAT-Cre*/+;*fl*/*fl* animals died before P30 (Fig. 6i) with significant loss of motor neurons (Fig. 6j). Therefore, we conclude that the effect of *Clcc1* loss-of-function in motor neuron loss is cell-autonomous.

Discussion:

Here, we characterized CLCC1 as a pore-forming component of an ER anion channel, activity of which is inhibited by luminal Ca^{2+} but facilitated by PIP2. We link rare *CLCC1* mutations to ALS and demonstrate that the ALS-associated mutations impair CLCC1 channel activity, damage ER ion homeostasis, and promote ER stress in brain, implying that disruption of ER ion homeostasis maintained by CLCC1 underlies etiology of ALS.

In the ALS Chinese cohort, S263R was found in two unrelated patients, suggesting it is a potential disease-causing mutation. Physically, S263 and W267 are in close proximity (Fig. 1d). Functionally, both S263R and W267R lead to the biological consequences to a similar extent (Fig. 1e, 1f, 2f, 3d, and 4f), suggesting they impair CLCC1 channel function probably through a similar mechanism. Like ALS-associated S263R and W267R mutations, K298A leads to similar phenotypes (Fig. 5), supporting the notion that impairment of ER ion homeostasis maintained by CLCC1 leads to neurodegeneration. Phenotypic analysis from five *Clcc1* alleles, including the two ALS alleles we generated, revealed that severity of CLCC1 mutant phenotypes is truly dose-dependent *in vivo* (Extended Data Fig. 14), which are evidenced *in vitro* by the effects of *CLCC1* knockdown dosage-dependently impairing ER volume, ER Ca^{2+} content, and steady state $[Ca^{2+}]_{ER}$ (Fig. 3 and 4). Given that CLCC1 is ubiquitously expressed [18], CLCC1 ER functions

469 described here, including maintenance of steady-state $[Cl^-]_{ER}$ and morphology and
470 regulation of ER Ca^{2+} homeostasis, could be applied to non-neuronal tissues and
471 cell types.

472 During internal Ca^{2+} release, both Cl^- efflux through ER anion channel(s) and
473 K^+ influx through either TRIC family channels [12] or RyRs/IP3Rs [8,15,40] are
474 indispensable for neutralization of membrane charge and balance of luminal
475 osmolarity at the same time (Extended Data Fig. 15). Upon depletion/dysfunction
476 of CLCC1, ER Ca^{2+} release was impaired (Fig. 4) and we speculate that it was
477 caused by Cl^- through CLCC1 no longer compensating for the membrane charge.
478 Therefore, double the amount of K^+ influx through ER cation channels was needed
479 to partially neutralize the membrane potential induced by Ca^{2+} release, which in
480 turn increases luminal osmolarity. In addition to this acute effect, CLCC1
481 maintains ER anion homeostasis and depletion of CLCC1 increases $[Cl^-]_{ER}$ (Fig.
482 3), which even worsens luminal osmolarity and ER swelling (Extended Data Fig.
483 15). Decreased CLCC1 dosage-dependently lowers ER Ca^{2+} content (Fig. 4g-4i),
484 which together with increased ER volume further decrease steady state $[Ca^{2+}]_{ER}$
485 (Fig. 4j and 4k) and damage Ca^{2+}-dependent protein folding capability, eventually
486 leading to ER stress, misfolded protein accumulation, and neurodegeneration [41]
487 (Extended Data Fig. 15).

CLCC1 shares little sequence similarity with any known ion channel, indicating that it belongs to a new channel family, therefore, we suggest renaming it ER anion channel 1 (ERAC1). Luminal Ca^{2+} inhibition on the channel activity prompts us to speculate a pre-inhibition mechanism in the resting state. However, when Ca^{2+} releases from ER, the local luminal [Ca^{2+}] drops sharply, which in turn relieves the inhibition (Extended Data Fig. 15). CLCC1 channel activity is facilitated by PIP2 (Fig. 5), reminiscent of PIP2 positive regulation of TRIC channel activity [34]. Amplification of both CLCC1 and TRIC channel conductance by PIP2 may have biological relevance to large Ca^{2+} conductance of RyRs/IP3Rs during internal Ca^{2+} release [8,40]. CLCC1 channel activity is insensitive to voltage (Fig. 2d) but sensitive to DIDS (Extended Data Fig. 6b and 6c), reminiscent of some early reported chloride currents recorded from SR/ER membrane preparation [13,42-44], but different from previously described CLCC1 currents [19]. Purified C350F mutant CLCC1 restored both MTSET- and DIDS-mediated cytoplasmic side modulation on channel activity (Fig. 2h and Extended Data Fig. 6b and 6c), suggesting that C350 that lies at the end of predicated TM3 is close to CLCC1 anion permeation pathway.

In K298A/+ mouse colony, K298A heterozygous mutation increased penetrance in disease progression by affecting expression of both mutant and wildtype CLCC1 (Extended Data Fig. 13), which form protein complex (Extended

Data Fig. 11c). Decreased CLCC1 is likely mediated by ER-associated degradation (ERAD) pathway, a cellular mechanism for ER protein quality control [45,46]. Cell-autonomous effect of *Clcc1* loss-of-function on ubiquitin-positive and mislocalized TDP-43 (Fig. 6) links *CLCC1* dysfunction to a common ALS pathology and its underlying disease mechanisms [37,47,48]. Dysfunction of RNA binding proteins (RBPs), including TDP-43, often leads to stress granule processing [38,39]. It will be intriguing to further investigate the crosstalk between ER and membraneless organelles, like stress granule [49], and how these dysfunctions in two cellular systems converge with the pathogenesis of ALS.

Acknowledgements:

We thank Drs. Jijie Chai, Jizong Wang and Jianping Wu for help with insect cell expression system, Ning Song, Mengyang Zhang, Atreyi Chakrabarty, Yan Han, and Feng Guo for technical assistance, Dr. Bingqing Xia for discussion of electrophysiology data, Dr. Haiteng Deng and Wenhao Zhang for sample analysis of mass spectrometry, Dr. Ying Li for TEM sample preparation and Hailong Lyu for movie production. We also thank the Protein Chemistry Facility at the Center for Biomedical Analysis of Tsinghua University. pCW-Cas9 was a gift from Eric Lander & David Sabatini (Addgene plasmid # 50661). LentiCas9-Blast was a gift from Feng Zhang (Addgene plasmid # 52962). We thank Dr. Susan Ackerman for the *NM*2453 mutant mouse line, Drs. Muming Poo, Songhai Shi, Wei Xiong, Wei Zhang, and Michael X. Zhu for comments on the manuscript, and Dr. Zhuan Zhou for comment on calcium imaging experiments. This work was supported by the Tsinghua-Peking Joint Center for Life Sciences, the Thousand-Talent Young Investigator Program, the IDG/McGovern Institute for Brain Research, the Personalized Medicines-“Molecular Signature-based Drug Discovery and Development” (Strategic Priority Research Program of the Chinese Academy of Sciences, Grant No. XDA12040221 and XDA15050308), the National Natural Science Foundation of China (81974197, 81371361, 31571097, 81773707,

82071426, 81873784, 61327014, 92049114 and 61175103), and the Shanghai Science and Technology Innovation Fund 15431901500.

Author contributions:

L.G. generated the CLCC1 N- and C-terminal antibodies, performed the biochemical experiments, immunofluorescence staining, and data analysis, and characterized the K298A, S263R and W267R knock-in mouse lines. Q.M. conducted planar phospholipid bilayer recording and data analysis. L.G., X.L., and B.X. performed calcium imaging. L.L. and X.P. generated the K298A, S263R, and W267R knock-in mouse lines. L.L. isolated the primary cardiomyocyte. J.H. and D.F. collected ALS sample and performed patient diagnosis and exome-sequencing. L.G., J.H., Z.G., and Y.J. wrote the manuscript. D.F., Z.G., and Y.J designed and supervised experiments.

Declaration of Interests:

The authors declare no competing interests.

References:

1 Cutting, G. R. Cystic fibrosis genetics: from molecular understanding to clinical application. *Nat Rev Genet* **16**, 45-56, doi:10.1038/nrg3849 (2015).

2 Duran, C., Thompson, C. H., Xiao, Q. & Hartzell, H. C. Chloride channels: often enigmatic, rarely predictable. *Annu Rev Physiol* **72**, 95-121, doi:10.1146/annurev-physiol-021909-135811 (2010).

3 Jentsch, T. J. & Pusch, M. CLC Chloride Channels and Transporters: Structure, Function, Physiology, and Disease. *Physiol Rev* **98**, 1493-1590, doi:10.1152/physrev.00047.2017 (2018).

4 Jentsch, T. J., Stein, V., Weinreich, F. & Zdebik, A. A. Molecular structure and physiological function of chloride channels. *Physiol Rev* **82**, 503-568, doi:10.1152/physrev.00029.2001 (2002).

5 Stauber, T. & Jentsch, T. J. Chloride in vesicular trafficking and function. *Annu Rev Physiol* **75**, 453-477, doi:10.1146/annurev-physiol-030212-183702 (2013).

6 Argenzio, E. & Moolenaar, W. H. Emerging biological roles of Cl- intracellular channel proteins. *J Cell Sci* **129**, 4165-4174, doi:10.1242/jcs.189795 (2016).

7 Gibson, A. *et al.* hCLCA1 and mCLCA3 are secreted non-integral membrane proteins and therefore are not ion channels. *J Biol Chem* **280**, 27205-27212, doi:10.1074/jbc.M504654200 (2005).

8 Fill, M. & Copello, J. A. Ryanodine receptor calcium release channels. *Physiol Rev* **82**, 893-922, doi:10.1152/physrev.00013.2002 (2002).

9 Clapham, D. E. Calcium signaling. *Cell* **131**, 1047-1058, doi:10.1016/j.cell.2007.11.028 (2007).

10 Berridge, M. J. The endoplasmic reticulum: a multifunctional signaling organelle. *Cell Calcium* **32**, 235-249 (2002).

11 Takeshima, H., Venturi, E. & Sitsapesan, R. New and notable ion-channels in the sarcoplasmic/endoplasmic reticulum: do they support the process of intracellular Ca2+ release? *J Physiol*, doi:10.1113/jphysiol.2014.281881 (2014).

12 Yazawa, M. *et al.* TRIC channels are essential for Ca2+ handling in intracellular stores. *Nature* **448**, 78-82, doi:10.1038/nature05928 (2007).

13 Miller, C. Voltage-gated cation conductance channel from fragmented sarcoplasmic reticulum: steady-state electrical properties. *J Membr Biol* **40**, 1-23 (1978).

14 Edwards, J. C. & Kahl, C. R. Chloride channels of intracellular membranes. *FEBS Lett* **584**, 2102-2111, doi:10.1016/j.febslet.2010.01.037 (2010).

15 Gillespie, D. & Fill, M. Intracellular calcium release channels mediate their own countercurrent: the ryanodine receptor case study. *Biophys J* **95**, 3706-3714, doi:10.1529/biophysj.108.131987 (2008).

16 Zsolnay, V., Fill, M. & Gillespie, D. Sarcoplasmic Reticulum Ca(2+) Release Uses a Cascading Network of Intra-SR and Channel Countercurrents. *Biophys J* **114**, 462-473, doi:10.1016/j.bpj.2017.11.3775 (2018).

17 al-Awqati, Q. Chloride channels of intracellular organelles. *Curr Opin Cell Biol* **7**, 504-508 (1995).

18 Jia, Y., Jucius, T. J., Cook, S. A. & Ackerman, S. L. Loss of Clcc1 results in ER stress, misfolded protein accumulation, and neurodegeneration. *J Neurosci* **35**, 3001-3009, doi:10.1523/JNEUROSCI.3678-14.2015 (2015).

19 Nagasawa, M., Kanzaki, M., Iino, Y., Morishita, Y. & Kojima, I. Identification of a novel chloride channel expressed in the endoplasmic reticulum, golgi apparatus, and nucleus. *J Biol Chem* **276**, 20413-20418, doi:10.1074/jbc.M100366200 (2001).

20 Lindholm, D., Wootz, H. & Korhonen, L. ER stress and neurodegenerative diseases. *Cell Death Differ* **13**, 385-392, doi:10.1038/sj.cdd.4401778 (2006).

21 Cook, C. & Petrucelli, L. Genetic Convergence Brings Clarity to the Enigmatic Red Line in ALS. *Neuron* **101**, 1057-1069, doi:10.1016/j.neuron.2019.02.032 (2019).

22 Taylor, J. P., Brown, R. H., Jr. & Cleveland, D. W. Decoding ALS: from genes to mechanism. *Nature* **539**, 197-206, doi:10.1038/nature20413 (2016).

23 Farhan, S. M. K. *et al.* Exome sequencing in amyotrophic lateral sclerosis implicates a novel gene, DNAJC7, encoding a heat-shock protein. *Nat Neurosci* **22**, 1966-1974, doi:10.1038/s41593-019-0530-0 (2019).

24 Vasilescu, J., Guo, X. & Kast, J. Identification of protein-protein interactions using in vivo cross-linking and mass spectrometry. *Proteomics* **4**, 3845-3854, doi:10.1002/pmic.200400856 (2004).

25 Suski, J. M. *et al.* Isolation of plasma membrane-associated membranes from rat liver. *Nat Protoc* **9**, 312-322, doi:10.1038/nprot.2014.016 (2014).

26 Akabas, M. H., Stauffer, D. A., Xu, M. & Karlin, A. Acetylcholine receptor channel structure probed in cysteine-substitution mutants. *Science* **258**, 307-310 (1992).

27 Matulef, K. & Maduke, M. Side-dependent inhibition of a prokaryotic ClC by DIDS. *Biophys J* **89**, 1721-1730, doi:10.1529/biophysj.105.066522 (2005).

28 Zhong, S., Navaratnam, D. & Santos-Sacchi, J. A genetically-encoded YFP sensor with enhanced chloride sensitivity, photostability and reduced ph interference demonstrates augmented transmembrane chloride movement by gerbil prestin (SLC26a5). *PLoS One* **9**, e99095, doi:10.1371/journal.pone.0099095 (2014).

29 Shcherbakova, D. M. & Verkhusha, V. V. Near-infrared fluorescent proteins for multicolor in vivo imaging. *Nat Methods* **10**, 751-754, doi:10.1038/nmeth.2521 (2013).

30 Jentsch, T. J. VRACs and other ion channels and transporters in the regulation of cell volume and beyond. *Nat Rev Mol Cell Biol* **17**, 293-307, doi:10.1038/nrm.2016.29 (2016).

31 Seidler, N. W., Jona, I., Vegh, M. & Martonosi, A. Cyclopiazonic acid is a specific inhibitor of the Ca2+-ATPase of sarcoplasmic reticulum. *J Biol Chem* **264**, 17816-17823 (1989).

32 de Juan-Sanz, J. *et al.* Axonal Endoplasmic Reticulum Ca(2+) Content Controls Release Probability in CNS Nerve Terminals. *Neuron* **93**, 867-881 e866, doi:10.1016/j.neuron.2017.01.010 (2017).

33 Suh, B. C. & Hille, B. Regulation of ion channels by phosphatidylinositol 4,5-bisphosphate. *Curr Opin Neurobiol* **15**, 370-378, doi:10.1016/j.conb.2005.05.005 (2005).

34 Yang, H. *et al.* Pore architecture of TRIC channels and insights into their gating mechanism. *Nature* **538**, 537-541, doi:10.1038/nature19767 (2016).

35 Suh, B. C. & Hille, B. PIP2 is a necessary cofactor for ion channel function: how and why? *Annu Rev Biophys* **37**, 175-195, doi:10.1146/annurev.biophys.37.032807.125859 (2008).

36 Rossi, J. *et al.* Melanocortin-4 receptors expressed by cholinergic neurons regulate energy balance and glucose homeostasis. *Cell Metab* **13**, 195-204, doi:10.1016/j.cmet.2011.01.010 (2011).

37 Lagier-Tourenne, C., Polymenidou, M. & Cleveland, D. W. TDP-43 and FUS/TLS: emerging roles in RNA processing and neurodegeneration. *Hum Mol Genet* **19**, R46-64, doi:10.1093/hmg/ddq137 (2010).

38 Renton, A. E., Chio, A. & Traynor, B. J. State of play in amyotrophic lateral sclerosis genetics. *Nat Neurosci* **17**, 17-23, doi:10.1038/nn.3584 (2014).

39 Ling, S. C., Polymenidou, M. & Cleveland, D. W. Converging mechanisms in ALS and FTD: disrupted RNA and protein homeostasis. *Neuron* **79**, 416-438, doi:10.1016/j.neuron.2013.07.033 (2013).

40 Foskett, J. K., White, C., Cheung, K. H. & Mak, D. O. Inositol trisphosphate receptor Ca2+ release channels. *Physiol Rev* **87**, 593-658, doi:10.1152/physrev.00035.2006 (2007).

41 Braakman, I. & Bulleid, N. J. Protein folding and modification in the mammalian endoplasmic reticulum. *Annu Rev Biochem* **80**, 71-99, doi:10.1146/annurev-biochem-062209-093836 (2011).

42 Ran, S., Fuller, C. M., Arrate, M. P., Latorre, R. & Benos, D. J. Functional reconstitution of a chloride channel protein from bovine trachea. *J Biol Chem* **267**, 20630-20637 (1992).

43 Kourie, J. I., Laver, D. R., Junankar, P. R., Gage, P. W. & Dulhunty, A. F. Characteristics of two types of chloride channel in sarcoplasmic reticulum vesicles from rabbit skeletal muscle. *Biophys J* **70**, 202-221, doi:10.1016/S0006-3495(96)79564-4 (1996).

44 Tanifuji, M., Sokabe, M. & Kasai, M. An anion channel of sarcoplasmic reticulum incorporated into planar lipid bilayers: single-channel behavior and conductance properties. *J Membr Biol* **99**, 103-111 (1987).

45 Trombetta, E. S. & Parodi, A. J. Quality control and protein folding in the secretory pathway. *Annu Rev Cell Dev Biol* **19**, 649-676, doi:10.1146/annurev.cellbio.19.110701.153949 (2003).

46 Vembar, S. S. & Brodsky, J. L. One step at a time: endoplasmic reticulum-associated degradation. *Nat Rev Mol Cell Biol* **9**, 944-957, doi:10.1038/nrm2546 (2008).

47 Neumann, M. *et al.* Ubiquitinated TDP-43 in frontotemporal lobar degeneration and amyotrophic lateral sclerosis. *Science* **314**, 130-133, doi:10.1126/science.1134108 (2006).

48 Dugger, B. N. & Dickson, D. W. Pathology of Neurodegenerative Diseases. *Cold Spring Harb Perspect Biol* **9**, doi:10.1101/cshperspect.a028035 (2017).

49 Lee, J. E., Cathey, P. I., Wu, H., Parker, R. & Voeltz, G. K. Endoplasmic reticulum contact sites regulate the dynamics of membraneless organelles. *Science* **367**, doi:10.1126/science.aay7108 (2020).

Materials and methods:

Protein expression and purification.

The DNA fragments encoding mouse CLCC1-N (residues 12-200, NM_145543.2) and CLCC1-C (residues 355-539) were cloned into pET28A (Novagen) with an N-terminal 6 × His tag or into pMAL-cRI with an N-terminal MBP (maltose binding protein, NEB) tag. The recombinant CLCC1 were expressed in BL21 derivative Rosetta (DE3) at 37 °C overnight. After ultrasonic cell disruption, the recombinant proteins in the soluble fractions were purified by Ni-NTA resin (Qiagen) or amylose resin (NEB) and dialyzed overnight in 10 mM PBS solution. For insect expression system, the full-length mouse and human *CLCC1* (wildtype, C350F, K298A, and K298E, S263R and W267R) were cloned into pFastbac-1 (Invitrogen) with a C-terminal His_{10} tag. The bacmids were extracted from DH10 Bac bacteria and transfected into *Sf9* insect cells, which were grown in SFX-Insect cell culture medium (GE Healthcare) at 26 °C to generate and amplify baculovirus (Bac-to-Bac system, Invitrogen). About 200 ml of High Five insect cells (1×10^6 cells per ml SIM HF culture medium, Sino Biological Inc.) were infected by 4 ml baculovirus to express the recombinant proteins. The infected High Five cells were harvested 48 hours after infection and homogenized in the TBS lysis buffer [50 mM Tris-HCl pH 7.4, 150 mM NaCl, 1% *n*-Dodecyl-β-D-Maltopyranoside (DDM, Inalco), and protease inhibitor cocktail, including 2 μg/ml pepstatin A, 4 μg/ml aprotinin, 10

687 mg/ml 4-(2-Aminoethyl) benzenesulfonyl fluoride hydrochloride, 4 μg/ml bestatin，
688 4 μg/ml E-64，4 μg/ml leupeptin, and 1 mM phenylmethane sulphonylfluoride] on
689 ice for 30 strokes with Dounce homogenizer, and then rotated for additional 30
690 minutes. The cell debris was removed by centrifugation at 30,000 × g for 1 hour.
691 The supernatant was harvested carefully, added 10 mM imidazole, and incubated
692 with Ni-NTA resin (Qiagen). The resin was washed with TBS buffer containing
693 0.05% DDM and 100 mM imidazole. The proteins were eluted from beads with
694 TBS buffer containing 0.05% DDM and 300 mM imidazole. The resulting
695 proteins were treated with 2 mM DTT and incubated on ice for 30 minutes. The
696 final concentrated proteins were further purified by a size-exclusion
697 chromatography (Superose 6 Increase, GE Healthcare) in the TBS buffer
698 containing 0.025% DDM and 2 mM DTT. The positions of some standard
699 molecular weight markers shown in user manual (GE Healthcare) were used to
700 estimate the size of protein complex. The peak fractions were collected, frozen
701 in liquid nitrogen, and stored at -80 °C for electrophysiology studies.

702 **Planar bilayer lipid membrane recording.**

703 Lipid bilayers formed across an aperture 0.2 mm in diameter in a delrin cup, with
704 a mixture of phosphatidylcholine (PC), phosphatidylserine (PS) (Avanti Polar
705 Lipids) and phosphoethanolamine (PE) (Lipoid) in a weight ratio of 1:2:2. The
706 lipids were dissolved in *n*-decane (Sigma) at a concentration of 50 mg lipid/ml *n*-

707 decane. All solutions were buffered by 10 mM HEPES pH 7.4. The lipid bilayer
708 separated the *cis* (In) solution from the *trans* (Ex) solution (1.0 ml each) and the
709 purified wildtype CLCC1 and its mutant variants were added to the *cis* side of a
710 lipid bilayer membrane. The purified proteins were added at *cis* side and the
711 membrane potential represents the voltage potential at *trans* side. The single
712 channel currents were recorded by adding 3.5 μl of 1.8 mg/ml protein to the *cis*
713 side in asymmetric KCl solution (In/Ex, 150/15 mM) at indicated voltages. The
714 macroscopic currents were recorded by adding 20.0 μl of 1.8 mg/ml protein. The
715 membrane potentials were held at + 60 mV and then stepped to a prepulse from -
716 40 mV to +100 mV with 20 mV increments for 3 s to elicit currents. The channel
717 currents were recorded in a voltage-clamp mode using a Warner BC-535 bilayer
718 clamp amplifier (Warner Instruments) filtered at 1 kHz, 25 ºC. The currents were
719 digitized using pCLAMP 10.4 software (Molecular Devices). The single-channel
720 conductance was determined by fitting to Gaussian functions. Opening times
721 less than 0.5-1.0 ms were ignored. The theoretical equilibrium potential was
722 calculated using the Nernst equation. The open probability P_o = t /T, where t is
723 the total time that the channel is observed in the open state and T is the total
724 recording time. The ion selectivity was calculated using the Goldman-Hodgkin-
725 Katz flux equation.

a. Monovalent anion: $E_{rev} = -\frac{RT}{zF}\ln\frac{P_A[A]_o}{P_B[B]_i}$

b. Divalent anion: $E_{rev} = -\frac{RT}{F}\ln\left(\sqrt{\frac{4P_{SO4}[SO4]_o}{P_{Cl}[Cl]_i}} + \frac{1}{4} - \frac{1}{2}\right)$

To examine the inhibitory effects of [2-(trimethylammonium)ethyl] methanethiosulfonate bromide (MTSET) and 4,4'-Diisothiocyano-2,2'-stilbenedisulfonic acid (DIDS), a certain amount of stocks of the two drugs were added into either *cis* or *trans* chamber using pipette.

The generation and purification of CLCC1 polyclonal antibodies.

To generate CLCC1 polyclonal antibodies, the purified mCLCC1-N (residues 12-200) and mCLCC1-C (residues 355-539) tagged with MBP were used to immunize the rabbits (SPF Japanese white rabbit). The subcutaneous inoculation was given once two weeks at least 3 times (0.1 mg antigen in complete/incomplete Freund's Adjuvant/rabbit, Sigma). The rabbit anti-serum was collected and purified by NHS-activated Sefinose beads conjugated by His-tagged mCLCC1-N or mCLCC1-C. The resulting antigen-antibody complexes were washed with PBS containing 0.15% Triton X-100 to reduce non-specific binding. The polyclonal antibodies with high affinity were eluted from the Sefinose beads by 50 mM glycine (pH2.5), and neutralized to pH7.4 immediately with Tris-HCl buffer.

Microsome isolation and protease digestion.

The microsome isolation was performed as previously described with slight modifications [25]. The brains and the livers of wildtype mice (0.5 mg tissue each preparation) were disrupted by using Dounce homogenizer for 30 strokes in a working buffer (225 mM mannitol, 75 mM sucrose, and 30 mM Tris-HCl, pH 7.4) on ice. The nuclei and unbroken cells were removed by centrifugation at 1,000 × g for 10 minutes. The supernatants containing the plasma membrane (PM) and the endoplasmic reticulum (ER) fraction were harvested by a further centrifugation at 10,000 × g for 10 minutes. The final pellet was collected at 25,000 × g for 30 minutes and resuspended in the working buffer. All centrifugation steps were executed at 4 °C. Protease digestion assay was performed as previously reported with some modifications (PMID: 20826464). In brief, the isolated microsome vesicles were incubated at 25 °C for 30 minutes with trypsin (Sigma). The digestion was performed in the absence or presence of 0.1 % (v/v) Triton X-100 and stopped by adding anti-trypsin inhibitor for 10 minutes on ice.

Chemical cross-linking experiments.

Protein cross-linking experiments were performed according to the user instruction (Thermo Fisher Scientific). Briefly, for *in vitro* crosslink, the purified N- and C-CLCC1 were incubated with DSS (Thermo Fisher Scientific) for 30 minutes at 25 °C then followed by adding quenching buffer (1 M Tris-HCl, pH 8.0). We set the DSS concentration gradients ranged from 0 to 1 mM. For *in vivo* crosslink,

293FT cells were harvested and washed with PBS twice. The resulting cells were incubated with different concentration DSS at room temperature, and then treated with the quenching buffer.

ER [Cl^-] and [Ca^{2+}] measurement

For ER steady-state [Cl^-] measurement, we modified a previously reported Cl^- probe [28], by adding a signal peptide and an ER detention signal KDEL and fusing it with a monomeric DsRed. The resulting ratiometric ER Cl^- probe we named RaMoride^{ER}. Naïve 293FT or *CLCC1* knock-down cells were transfected with RaMoride^{ER} and then washed with HBSS buffer without calcium and magnesium. To validate RaMoride^{ER}, we suspended the cells with buffer containing 0.6 mM MgSO4, 38 mM sodium chloride, and 100 mM potassium chloride (20 mM Hepes, pH 7.4), or corresponding extracellular [Cl^-] ([Cl^-]$_{Extra}$) by replacement of Cl^- by gluconate. To estimate ER steady-state [Cl^-], the cells were suspended in HBSS buffer containing 2 mM Ca^{2+} and 140 mM Cl^-.

For ER steady state [Ca^{2+}] measurement, we transfected naïve 293FT or *CLCC1* knock-down cells with a previously reported ER-targeted low-affinity calcium probe [32]. The transfected cells were washed with HBSS buffer without calcium and magnesium, and then suspended with the following buffers separately: the HBSS solution containing 10 μM ionomycin (Beyotime) and 1mM EGTA for baseline (Fbaseline); the HBSS solution with 2 mM calcium chloride for steady-

785 state (Fsteady); the HBSS solution with 10 mM calcium chloride and 10 μM
786 ionomycin for saturating the probe (Fmax). The relative ER steady-state [Ca^{2+}]
787 was estimated by ΔFsteady (Fsteady-Fbaseline) divided by ΔFmax (Fmax-
788 Fbaseline). The fluorescent signals from individual cell were collected by
789 LSRFortessa flow cytometer (BD Biosciences). For Cl^- sensor and ER-GCaMP6-
790 210, we employed the FITC channel (488 nm); for DsRed, we employed PE
791 channel (561 nm). Data were analyzed by FlowJo X. The cells were treated
792 with 7-AAD (BioLegend) or DAPI (Beyotime) to exclude the dead cells.

793 **Transmission electron microscopy (TEM)**

794 Mice at P30 were perfused by 0.1 M phosphate buffer (PB, pH 7.4) at room
795 temperature, then fixed by fixation solution (FS, 4% PFA (W/V) in PB) and by 2.5%
796 glutaraldehyde in FS at 4 °C overnight. The similar regions of the cerebellums
797 were cut into 200 μm for embedding which was performed at the Center for
798 Biomedical Analysis of Tsinghua University. The images were taken by Tecnai
799 Spirit electron microscopy.

800 **Lentiviral shRNA knockdown and the inducible expression system.**

801 Lentiviruses were produced by co-transfecting 293FT cells with transfer constructs,
802 pMD2.G and psPAX2, by linear PEI (MW 25,000, Polysciences). The medium
803 containing lentivirus without debris was concentrated by centrifugation at 20,000
804 rpm for 2 hours and resuspended in PBS. For generation of the stable cell line

805 expressing human *CLCC1* shRNA (MissionRNAi, Sigma), the 293FT cells were
806 selected with 1 μg/ml puromycin. For construction of the inducible expression
807 system, we modified the pCW-cas9 (pCW-Cas9, Addgene #50661), in which the
808 *Cas9* was replaced by our target genes. After 48-hour drug resistant selection,
809 the cells were maintained in medium containing appropriate antibiotics and used
810 within one week. The knockdown efficiency and inducible expression of our
811 interested proteins were examined by western blot. For exogenous wildtype and
812 mutant CLCC1 expression induction, 1 μg/ml Dox (Sigma) was applied in culture
813 medium.

814 **Cell culture and Calcium imaging.**

815 293FT and Hela cells were maintained in Dulbecco's modified Eagle's medium
816 (DMEM) supplemented with 10% heat-inactivated Fetal Bovine Serum (FBS) and
817 1% penicillin/streptomycin (GE Healthcare). The primary cardiomyocyte culture
818 was performed as previously reported (PMID: 24056408). Briefly, the hearts from
819 P2 neonatal mice were dissected and minced in the Ca^{2+} and Mg^{2+} free PBS
820 supplemented with 20 mM BDM (Sigma). The chopped tissues were digested in
821 PBS containing 0.125% (w/v) trypsin at 4 °C for 2 hours followed by the digestion
822 of 0.5% collagenase I (Sigma) at 37 °C for 30 minutes. After the digestion, the
823 cardiomyocytes were seeded on gelatin (Sigma)-coated cover slips and in
824 DMEM/F12 medium containing 10% FBS. After 48 hours, the cardiomyocytes

showed spontaneous beating, which were used in calcium imaging experiments. For calcium imaging, the 293FT cells or cardiomyocytes seeded on the coverslips were loaded with the ratiometric Ca^{2+} indicator (Fura-2 AM, Thermo Fisher Scientific) in Krebs-Ringer-Hepes (KRH) buffer (25 mM HEPES pH7.4, 125 mM NaCl, 6 mM glucose, 5 mM KCl, 1.2 mM $MgCl_2$) supplemented with detergent Pluronic F-127 (Thermo Fisher Scientific). After 30-minute loading at room temperature in dark, the coverslip was washed twice with KRH buffer and then subjected to calcium imaging in a perfusion chamber on an inverted Nikon TiE microscope with 20 × Fluar objective. The Metafluor Program software (Molecular Devices) was used to monitor and calculate the real time changes of calcium concentration in cytoplasm.

Western blot, immunoprecipitation, and immunostaining.

For western blot and immunoprecipitation (IP), the cultured cells or tissues were lysed in the TBS lysis buffer (50 mM Tris-HCl pH 7.4, 150 mM NaCl, 1% DDM, and protease inhibitor cocktail). After incubation for 20 minutes on ice, the cell debris was removed by centrifugation at 13,000 × g for 5 minutes. For western blot, the supernatant was boiled with 2 × SDS loading buffer and the proteins were separated on SDS-PAGE gel and transferred to PVDF membrane (GE Healthcare) using standard protocol. The blot was incubated with the primary antibody overnight at 4 °C, and then HRP-conjugated secondary antibody RT for 60 minutes.

For IP assay, the Dynabeads (Invitrogen) were used to capture the tagged target proteins. The beads were washed with the TBS lysis buffer and pre-incubated with the primary antibody at room temperature for 20 minutes then incubated with the supernatant of the cell lysate at 4 °C for at least 3 hours or overnight. The beads were washed five times with washing buffer (50 mM Tris-HCl pH 7.4, 150 mM NaCl, 0.025% DDM, and protease inhibitor cocktail). The IPed proteins were eluted by 2 × SDS-loading buffer at 95 °C for 5 minutes. For cultured cell immunostaining, the cultured Hela cells were fixed with 4% (W/V) paraformaldehyde (PFA) and permeabilized by 0.3% Triton X-100 in PBS for 10 minutes. The fixed cells were blocked with blocking buffer (PBS with 3% BSA) and stained with primary antibody overnight at 4 °C, then incubated with secondary antibody for 1 hour at room temperature. For tissue immunostaining, the PFA fixed paraffin-embedded sections were deparaffinized with standard protocol as described previously [18]. For antigen retrieval, the section was boiled in the sodium citrate buffer (10 mM sodium citrate, pH 6.0) and cooled to room temperature. After antigen retrieval, the sections were blocked with the blocking buffer and stained with the primary and secondary antibodies. For antibodies, the following primary antibodies were used, including anti-FLAG (1:5000, clone 3B9 mouse, Abmart), anti-Myc (1:5000, clone 19C2 mouse, Abmart), anti-tubulin (1: 10,000, clone B-5-1-2 mouse, Sigma), anti-calmodulin binding protein (1: 2,000, rabbit, Millipore), anti-Bip (1:300, rabbit, Abcam), anti-ubiquitin (1:200, P4D1

mouse, Cell Signaling Technology), anti-His (1:1000, rabbit, Cell Signaling Technology), and anti-GAPDH (1:5000, 14C10 rabbit, Cell Signaling Technology). For secondary antibodies, we used Alexa-conjugated secondary (488, 555) antibodies (Life Technologies; Molecular Probes) at 1:500 and HRP-linked secondary antibodies (GE Healthcare) at 1: 5,000.

Generation of the knock-in (KI) and *Clcc1* floxed mouse and genotyping.

For the generation of the KI mouse line, we synthesized the DNA oligo which carried the target mutations. The gRNA (ttggttggttccaccaacaaAGG for K298A, tggattggactggaagtctcTGG for S263R, and ttggcatgggtcatccttatAGG for W267R, PAM sites capitalized) was generated by *in vitro* transcription (Invitrogen). The donor DNA oligo, gRNA, and *Cas9* mRNA were injected into C57BL/6J embryos. The injected embryos were transferred into the oviduct ampulla of the pseudo-pregnant ICR (JAX, Stock No. 009122) female recipients. The right genotype offsprings were backcrossed to C57BL/6J for at least three generations to establish the line. For genotyping the K298A KI mouse, the gDNA PCR (forward primer: ggcacagtcaaaaccaaactgatcttg and reverse primer: gagcctaaaaccaaagaccagagc) products were digested with MspA1I (NEB). Primers for the S263R KI mice (forward primer: ggatttgcgttcccagctcggtt and reverse primer: tccgtccctttaactttgaggcag) and for the W267R KI mice (forward primer: gtgggcacagtcaaaaccaaactga and reverse primer:

886 gagcctaaaaccaaagaccagagca). The gDNA PCR products confirmed by Sanger
887 sequencing. The animal facility at Tsinghua university has been fully accredited
888 by the Association for the Assessment and Accreditation of Laboratory Animal
889 Care International (AAALAC) since 2014. All animal protocols were approved by
890 the Institutional Animal Care and Use Committee (IACUC) at Tsinghua university
891 based on Guide for the Care and Use of Laboratory Animals (Eighth Edition, NHR).
892 *Clcc1* floxed mouse were generated by Cyagen (China). Two loxP sites were
893 inserted the intron 6 and 7 by CRISPR/Cas9, respectively. The founders were
894 backcrossed to C57BL/6J mice for at least three generations to reduce off-target
895 effect.

896 **Molecular Biology.**

897 The following sequences of CLCC1 homologues from different vertebrate species
898 were obtained from the NCBI GenBank: *Homo Sapiens* (NM_001048210.2), *Mus*
899 *musculus* (NM_145543.2), *Pan troglodytes* (XM_009426847.2), *Rattus norvegicus*
900 (NM_133414.1), *Gallus gallus* (XM_422186.5), *Anolis carolinensis*
901 (XM_003223596.3), *Xenopus tropicalis* (XM_002932173.4), *Danio rerio*
902 (XM_002667211.5). The alignment result was done by using the Clustal W
903 program and reported from http://espript.ibcp.fr/ESPript/cgi-bin/ESPript.cgi (PMID:
904 24753421).

905 **Mass Spectrometry.**

Brain lysate of K298A/*NM* mice were applied for IP with CLCC1-C antibody. Gel bands between 55 kD and 100 kD from the IP were excised for ingel digestion, and the WT and K298A CLCC1 small peptides were identified by mass spectrometry (MS) as previously described (PMID: 24563215). Briefly, proteins were disulfide reduced with 25 mM dithiothreitol (DTT) and alkylated with 55 mM iodoacetamide. In-gel digestion was performed using sequencing grade-modified pepsin in 1% Fomic Acid at 4 °C for 30min. The peptides were extracted twice with 1% trifluoroacetic acid in 50% acetonitrile aqueous solution for 30 min. For LC-MS/MS analysis, peptides were separated by Thermo-Dionex Ultimate 3000 HPLC system. The analytical column was a homemade fused silica capillary column (75 μm ID, 150 mm length; Upchurch, Oak Harbor, WA) packed with C-18 resin (300 A, 5 μm; Varian, Lexington, MA). Mobile phase A consisted of 0.1% formic acid, and mobile phase B consisted of 100% acetonitrile and 0.1% formic acid. MS/MS spectra from each LC-MS/MS run were searched against the user defined database using Proteome Discoverer (Version 1.4) searching algorithm. High confidence score filter (FDR < 1%) was used to select the “hit” peptides and their corresponding MS/MS spectra were manually inspected.

Human subjects, whole-exome sequencing (WES), and filtering of causative mutations.

701 sporadic ALS patients were enrolled from the Department of Neurology of Peking University Third Hospital from 2007-2020. All ALS cases were diagnosed as possible, probable, or definite ALS according to the revised EI Escorial criteria. Clinical information, including age, sex, age of onset, site of onset, disease duration, family history and neurologic examination, were recorded. 1990 control samples for DNA analysis were obtained from the same hospital with no diagnosis of a neurological disorder. All subjects have signed the informed consent forms and this study was approved by the Ethics Committee of Peking University Third Hospital. For WES, DNA was isolated from peripheral blood using DNA Isolation Kit (Bioteke, AU1802). Genomic DNA (1μg) were fragmented into 200-300bp length by Covaris Acoustic System. The DNA fragments were then processed by end-repairing, A-tailing and adaptor ligation (Agilent SureSelect Human ALL Exon, V6), a 4-cycle pre-capture PCR amplification, targeted sequences capture. Captured DNA fragments were eluted and amplified by post capture PCR. The final products were sequenced with 150-200bp paired-end reads on Illumina HiSeq X platform according to the standard manual. The raw data produced on HiSeq X were filtered and aligned against the human reference genome (hg19) using the BWA Aligner (http://bio-bwa.sourceforge.net/,v0.7.15). The single-nucleotide polymorphisms (SNPs) were called by using GATK software (Genome Analysis Toolkit, v3.6). Variants were annotated using ANNOVAR (annovar.openbioinformatics.org/en/latest/). All variants found by the WES were

946 further confirmed by the Sanger sequencing. Variants were filtered for presence
947 of nonsynonymous heterozygous variants with a minor allele frequency<1% in the
948 Exome Aggregation Consortium (ExAC) database (http://exac.broadinstitute.org/),
949 the Exome Sequencing Project (ESP) (http://evs.gs.washington.edu), the 1000
950 Genomes Project (1000G) database (http://www.1000genomes.org/) and the
951 Genome Aggregation Database (gnomAD) (http://gnomad.broadinstitute.org/).
952 To identify the functional effect of the mutations, in silico predictive programs were
953 performed, including Polyphen-2 (http://genetics. bwh.harvard.edu/pph2), SIFT-2
954 (http://sift.jcvi.org) and Mutation Taster (http:// mutationtaster.org). The genomic
955 evolutionary rate profiling scores were acquired by GERP++ program
956 (http://mendel.stanford.edu/SidowLab/downloads/gerp/index. html).

957 **Quality control (QC)**

958 After the variants were called and annotated, we applied QC steps to individuals
959 and variants. Briefly, individual-level QC was based on common single
960 nucleotide polymorphisms (SNPs) (minor allele frequency MAF> 1%) with a
961 genotype call rate > 95%. We excluded individuals from the association analysis
962 who (1) were sex-discordant/ambiguous (43 individuals, 17 ALS cases and 26
963 controls); (2) presented a genotyping call rate < 80% (0 individuals); (3) exhibited
964 an excessive heterozygosity rate (> 3 SD from the mean; 36 individuals, 2 cases
965 and 34 controls); (4) were shown to be ancestry outliers based on the three

966 principal components (PCs) derived from common SNPs (0 individuals); or (5)
967 exhibited a genetic relationship matrix value > 0.1 with another individual (32
968 individuals, 12 ALS patients and 20 controls). After the QC procedures, a total of
969 670 ALS cases and 1910 controls remained for the analyses. We performed the
970 same QC steps on the common capture set. After obtaining clean sets of
971 individuals, we excluded genetic variants based on the following criteria: (1) a low
972 genotype call rate < 99%; (2) deviation from Hardy–Weinberg equilibrium in
973 controls ($p < 10^{-6}$); (3) differential missingness between cases and controls ($p <$
974 10^{-6}).

975 **Gene-based burden analysis**

976 We assessed the evidence of an excess of rare damaging mutations in the ALS
977 cases compared to the controls at the gene level using the sequence kernel
978 association test (SKAT)-O implemented in the R SKAT package. We used SKAT-
979 O because it optimally combines the burden test (which is most powerful when a
980 high proportion of variants in a gene are causal and exhibit the same direction of
981 effect) with SKAT (which is best used when only a small proportion of variants in
982 a gene are causal or if both risk and protective variants are present). Briefly, we
983 analyzed RefSeq genes with damaging singleton sets [23]: missense variants with a
984 MAF lower than 0.01% (in our dataset and East Asian populations from databases
985 including 1000G, ESP and gnomAD non-neuro subset), and with an allele count

(AC) of 1 in our data. The SKAT-O results were corrected for sex and the top ten PCs based on HapMap3 SNPs. We used the default settings in the R SKAT package, including the imputation of missing genotypes and resampling methods for computing *p* values.

END.

Figures

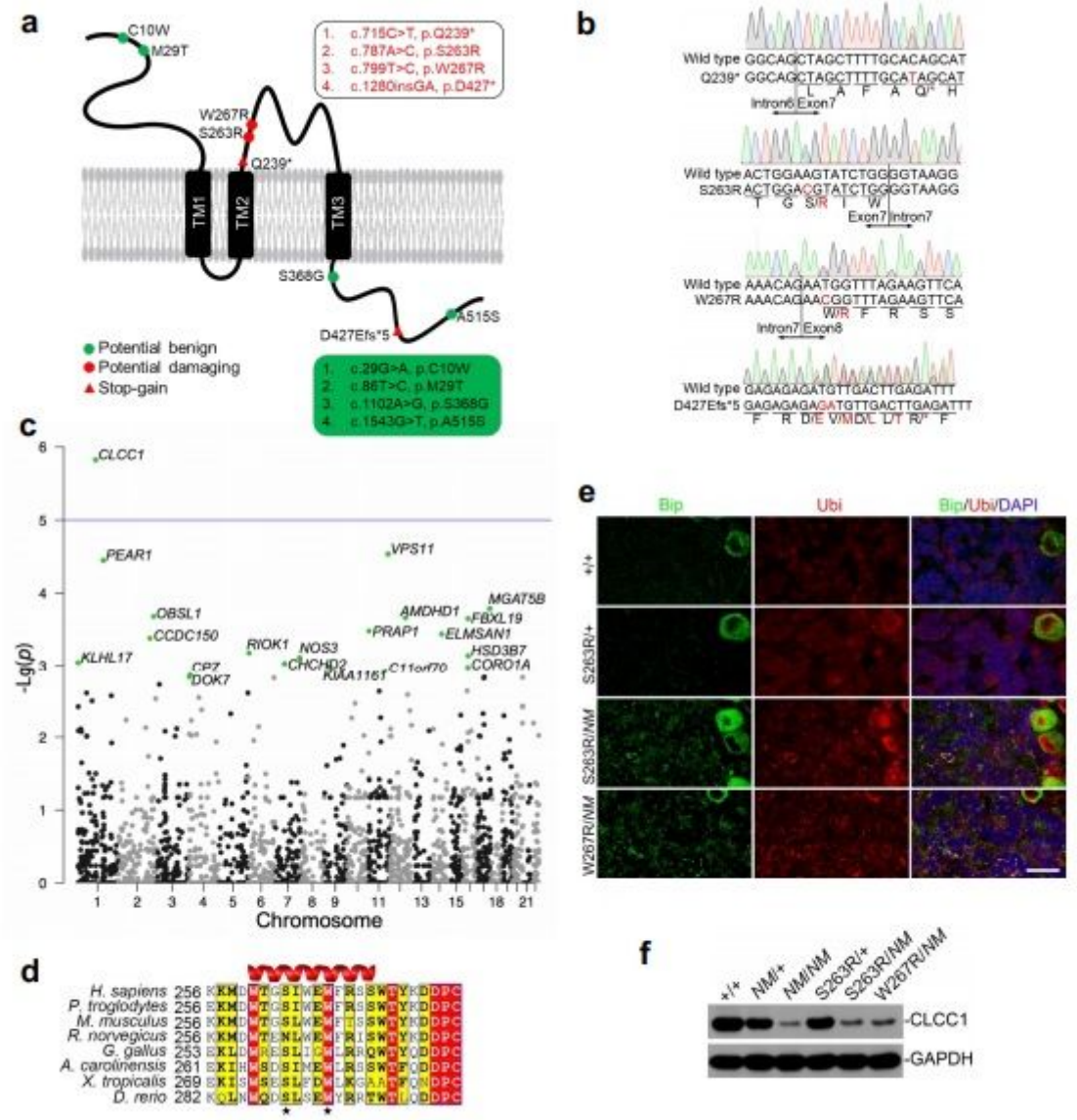

Figure 1

ALS-associated CLCC1 mutations S263R and W267R reduce mutant CLCC1 expression and promote ER stress in vivo. a, The nonsynonymous (colored circle) and stopgain (red triangle) mutations of CLCC1 were identified in a Chinese sporadic ALS cohort. The potential damaging mutations are labeled in red. b, Validation of the potential diseasecausing mutations of CLCC1 by Sanger sequencing. Genomic DNA extracted from peripheral blood cells of individual ALS patients. The PCR products were subject to Sanger sequencing and the boundaries of adjacent exon and intron are marked. c, The Manhattan plot for an exome-wide rare variant burden analysis. The p value of CLCC1 (1.51×10-6, with OR = 5.72). d, A protein alignment of CLCC1 encompassing S263, W267, and neighboring residues. Note that S263 and W267 are located in a predicted alpha helix. e, ER stress and misfolded protein accumulation documented by Bip and ubiquitin (Ubi) staining in cerebella of compound heterozygous mice (S263R/NM and W267R/NM).

NM, the NM2453 allele is an IAP (intracisternal A-particle) insertion in the intron 2 of Clcc1, which greatly reduces the expression of CLCC1 protein to ~10% of that in wildtype animals (PMID: 25698737). S263R/+ and wildtype (+/+) are negative for the phenotypes. f, Cerebellar expression of CLCC1 in the indicated genotypes. Both S263R and W267R lowered the expression of CLCC1. GAPDH, loading control. In e and f, +/+, 1.5 month; other genotypes, P35. Scale bar in E, 20 μm

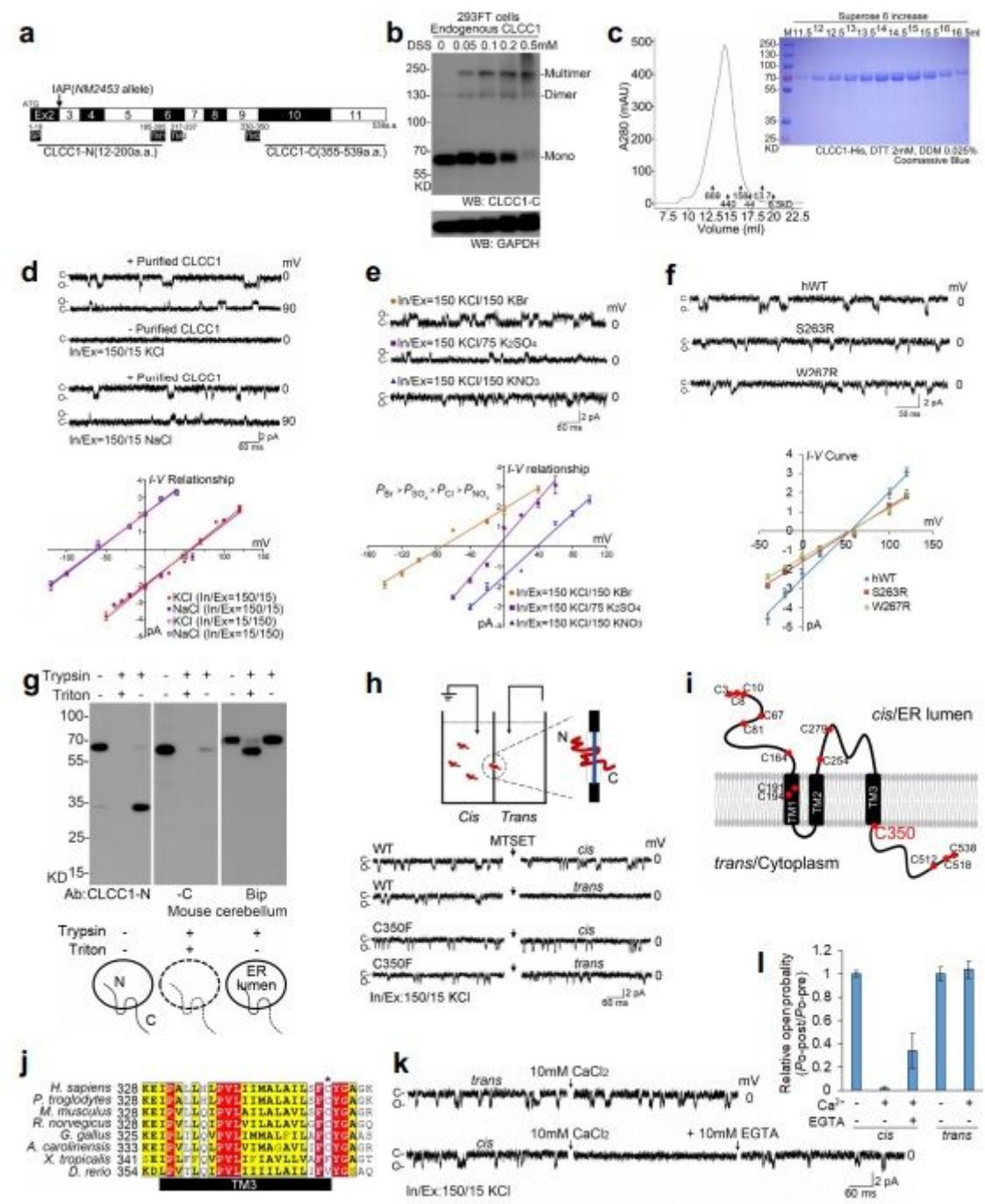

Figure 2

CLCC1 is a pore-forming component of an ER anion channel and luminal Ca2+ inhibits the channel activity. a, Domain prediction of mouse CLCC1 (mCLCC1) that contains a signal peptide (SP) and three

transmembrane segments (TMs). mCLCC1 is encoded by 10 exons (Ex2-11) (NM_145543.2). Note the N-terminal (12-200 a.a.) and Cterminal polypeptides (355-539 a. a.) used for generation of the N- and C-terminal antibodies, respectively. b, Naive 293FT cells were treated with disuccinimidyl suberate (DSS) at indicated concentrations. Cell lysates were separated by SDS-PAGE and blotted with CLCC1 C-terminal antibody (CLCC1-C). c, Chromatograph of His-tagged mCLCC1 expressed by an insect expression system and purified by Nickel column. Standard molecular weight markers are indicated by arrows. d, Purified mCLCC1 from (c) were incorporated into planar phospholipid bilayer and single channel currents were recorded in asymmetric KCl and NaCl solutions at indicated voltages (upper). C, closed state; O, open state. Current-voltage (I-V) relationships in asymmetric KCl and NaCl solutions (lower). e, Single channel currents recorded at 0 mV with 150 mM KCl in cis and 150 mM KBr, 75 mM K_2SO_4, or 150 mM KNO_3 in trans (upper). I-V relationships under conditions (lower). f, Single channel activities (upper) and I-V relationships (lower) recorded from planar bilayers with purified human wildtype (hWT), S263R, and W267R mutant CLCC1, respectively. Solution, asymmetric KCl (In/Ex, 150/15 mM). In d, e, and f, values are presented as mean ± SEM ($n \geq 6$). g, Topology of CLCC1 determined by microsome preparation. Microsomal vehicles prepared from mouse cerebellum were treated with trypsin alone, or trypsin together with Triton X-100. Protein lysates were then separated by SDS-PAGE and probed with CLCC1 N- and C-terminal antibodies. As a control, Bip, an ER lumen resident, was protected from trypsinization. h, Application of 2 mM MTSET in trans but not cis side blocked mCLCC1 channel activity. We defined cis side as the chamber we applied purified CLCC1 proteins (upper). The C350F mCLCC1 mutant was resistant to MTSET ($n \geq 6$). i, Cysteine residues of CLCC1, with C350 highlighted. j, An alignment of predicted TM3 of CLCC1 across different species. C350 is labeled with an asterisk. Note the corresponding residue of Homo sapiens and Mus musculus C350 is phenylalanine in Xenopus. k, Application of 10 mM $CaCl_2$ in cis but not trans reduced mCLCC1 channel activity. The inhibitory effect of Ca^{2+} was partially prevented by EDTA (10mM). l, Statistical analysis of normalized relative open probability (Po). Relative Po, Po-post/Po-pre, Po after $CaCl_2$ or EDTA treatment divided by that before the treatment. Values are presented as mean ± SEM ($n = 6$).

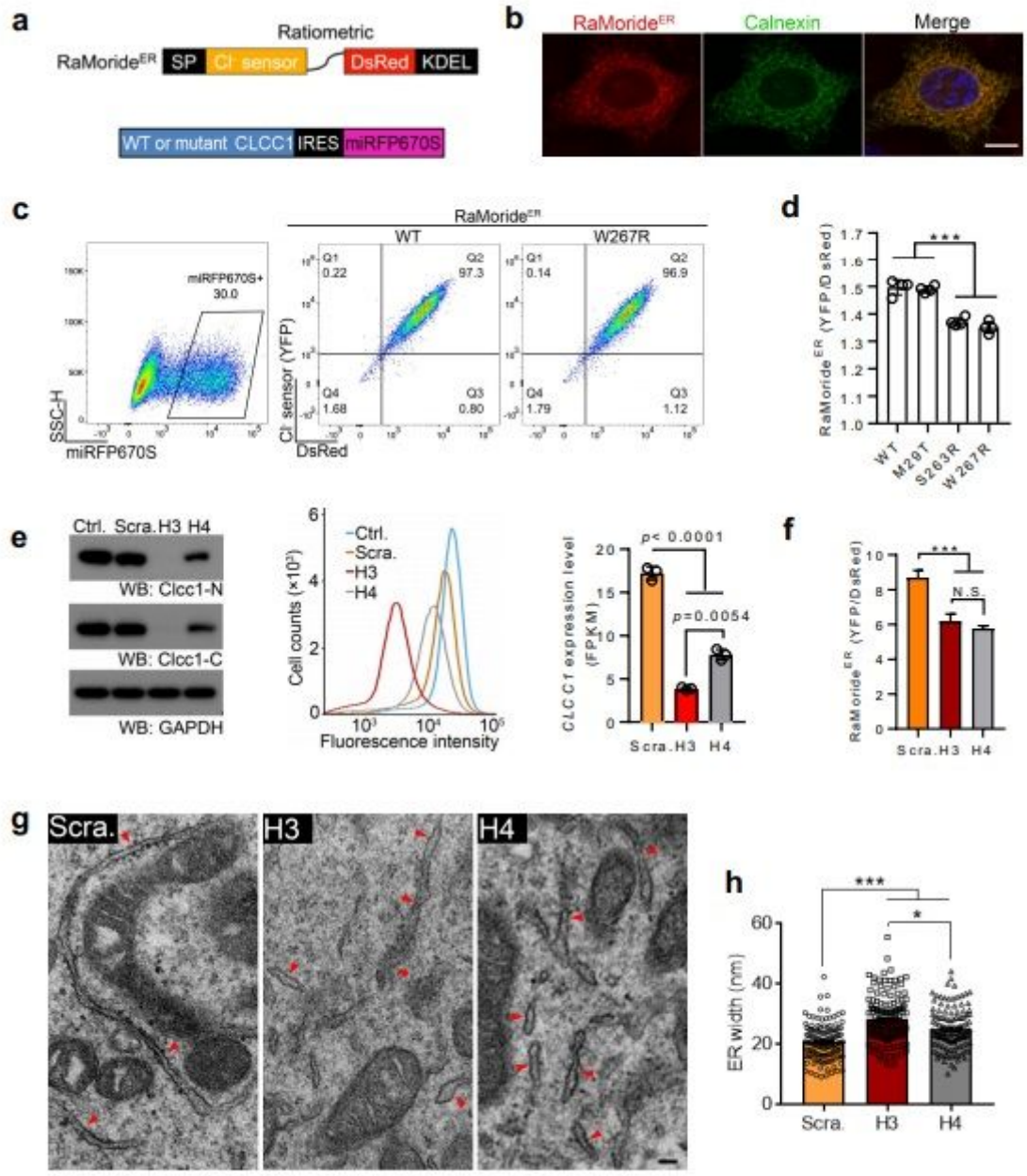

Figure 3

Dysfunction of CLCC1 impairs steady state [Cl-]ER and leads to ER swelling. a, Ratiometric Cl- sensor (RaMorideER) for ER [Cl-] ([Cl-]ER) measurement. A signal peptide (SP) was tagged to the N-terminus of a previously reported Cl- sensor (PMID: 24901231), which was then fused to a monomeric DsRed as an internal control for the probe expression level and an ER retention signal (KDEL) at the C-terminal end. The resulting ratiometric Clsensor (RaMorideER) for ER [Cl-] ([Cl-]ER) measurement (upper). Cell expressing wildtype (WT) or ALS-associated mutant CLCC1 was monitored by the expression of an engineered near-infrared fluorescent protein, miRFP670S (PMID: 23770755). IRES (Internal Ribosome Entry Sites) sequences were employed to ensure the co-expression (lower). b, ER localization of RaMorideER, showing a prominent overlap of the DsRed fluorescence with Calnexin immunostaining signals. c and d, Measurement of [Cl-]ER in 293FT cells expressing WT or ALS-associated mutant CLCC1

by RaMorideER. [Cl-]ER was reflected by the ratio of YFP/DsRed fluorescent signals. Cells expressing WT or ALS-associated mutant CLCC1 were sorted by miRFP670S. Representative FACS (Fluorescence Activated Cell Sorting) plots (c) and the summary data (d) are shown. e, Knockdown of CLCC1 in 293FT cells infected with lentiviral H3 and H4 shRNAs, measured by western blot (left), FACS (middle), and RNA-seq (right). Ctrl., MOCK control; Scra., scrambled shRNA; H3 and H4, shRNAs specific for CLCC1. f, Steady state [Cl-]ER measured by RaMorideER in 293FT cells infected with the indicated shRNAs. g and h, Transmission electron microscopy (TEM) images of 293FT cells infected with the indicated shRNAs. Ribosome-bound rough ER was marked by red arrows. ER width was calculated and the summary data are shown in (h). In d, f, and h, values are presented as mean ± SEM from at least three independent experiments or biological replicates; N.S., no significant difference, *p<0.05, **p<0.01, ***p

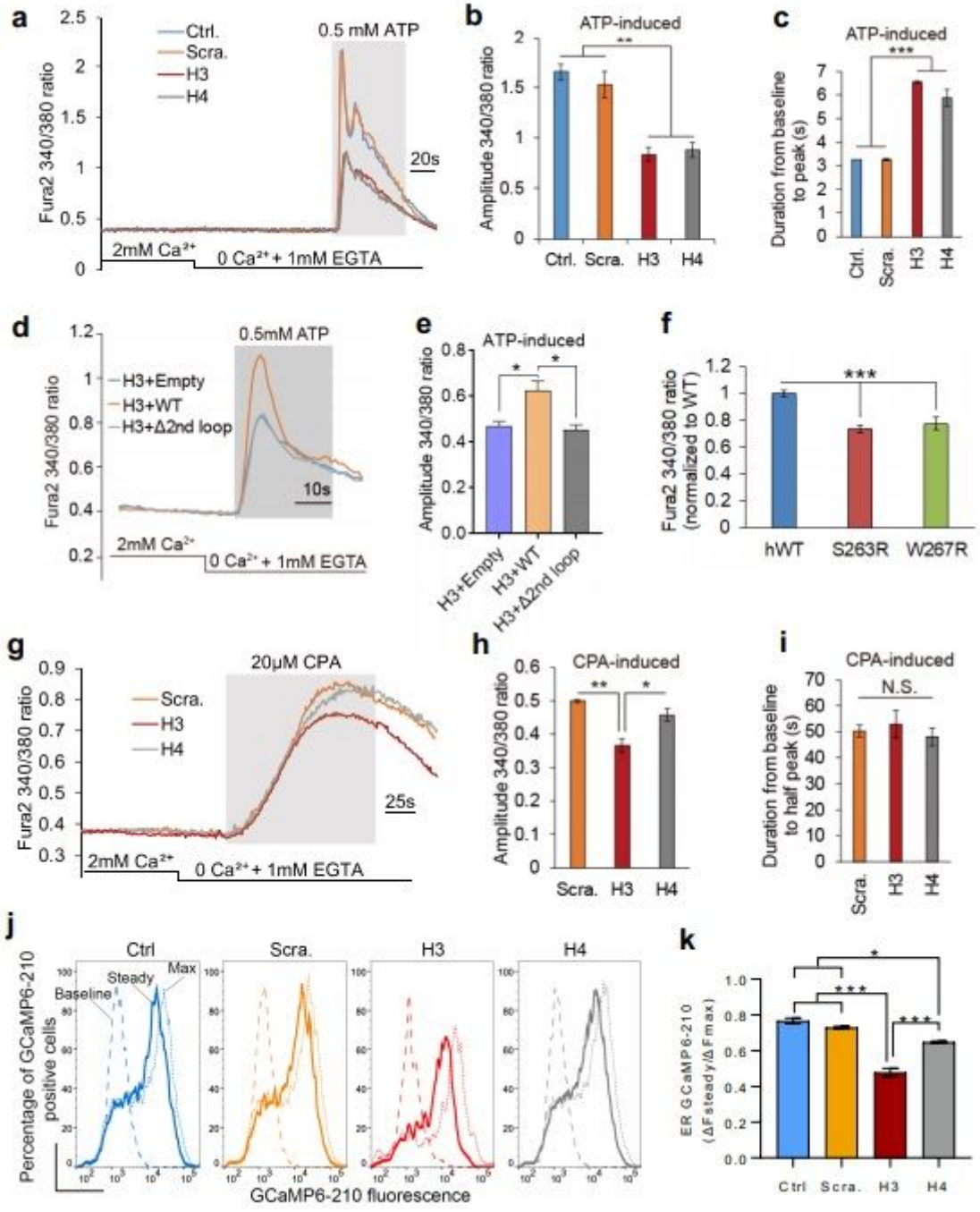

Figure 4

Dysfunction of CLCC1 impairs internal Ca2+ release and depletion of CLCC1 dosage-dependently reduces [Ca2+]ER. a-c, 293FT cells infected with the indicated shRNAs were loaded with Fura-2 and stimulated with ATP in a calcium-free medium (gray rectangle). Representative Ca2+ release traces averaged from at least 50 cells (a). The knockdown of CLCC1 reduced the amplitude (b) but increased the time-to-peak (c) of ATPinduced Ca2+ release. d and e, Full-length WT mCLCC1 but not the Δ2nd loop mutant CLCC1 restored the ATP-induced Ca2+ release damaged by H3 shRNA knockdown. The data summary shown in (e). f, ATP-induced internal Ca2+ release was impaired by S263R and W267R mutants. Human wildtype (hWT) and S263 and W267 mutant CLCC1 were expressed in 293FT cells. g-i, ER Ca2+ content was estimated by CPA-induced cytosolic Ca2+ rise in the calcium-free medium (gray rectangle) in 293FT cells infected with the indicated shRNAs. Shown are representative traces of CPA-induced calcium leak averaged from at least 50 cells (g) and summary data for the amplitude (h) and time-to-half peak (i) of CPA-induced cytosolic Ca2+ rise. j and k, Steady state [Ca2+]ER in 293FT cells infected with the indicated shRNAs was measured by fluorescent signals of ER-GCaMP6-210 a previously reported low affinity Ca2+ probe (PMID: 28162809) by FACS. Baseline, 1 mM EGTA + 10 μM ionomycin; Steady, normal medium containing 2 mM Ca2+; Max, 10 mM Ca2+ + 10 μM ionomycin. The summary data (k) were from three independent experiments. ΔFsteady = (Fsteady-Fbaseline); ΔFmax = (Fmax-Fbaseline). Values are presented as mean ± SEM. In b, c, e, f, h, and i, n > 150 cells pooled from three independent experiments. N.S., no significant difference, *p<0.05, **p<0.01, ***p

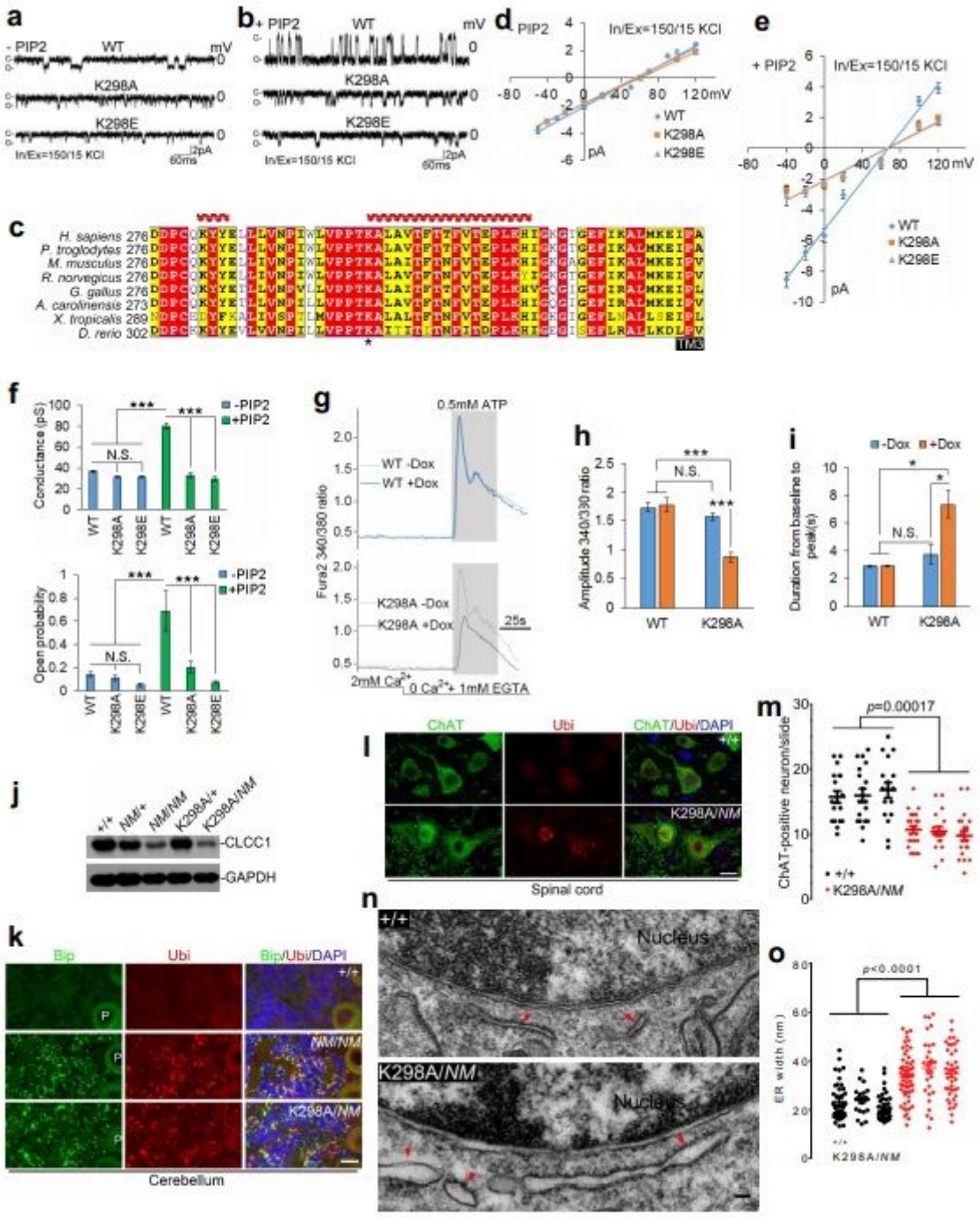

Figure 5

Mutation of K298 a PIP2-sensing residue for CLCC1 channel activity impairs ER Ca2+ release and promotes ER swelling and motor neuron degeneration. a and b, Single channel activities recorded after incorporating the purified wildtype (WT), K298A, and K298E mutant mCLCC1 into the planar phospholipid bilayer. In b, the phospholipid bilayer contained 2% PIP2. c, An alignment of sequences encompassing the 2nd loop of CLCC1 among different species. d and e, I-V relationships in the absence (d) and presence (e) of PIP2 for WT mCLCC1 and its K298A and K298E mutants recorded from planar phospholipid bilayer in

the asymmetric KCl solutions. f, Summary data of slope conductance (upper) and channel open probability (Po) at 0 mV (lower) in the asymmetric KCl solutions. g, A lentiviral inducible system was used to express wildtype mCLCC1 (WT) and its K298A mutant (K298A) in 293FT cells. ATP-induced Ca2+ release was measured in the calcium-free culture medium in Fura-2 loaded cells with (+Dox) or without (-Dox) induction. h and i, Summary data of amplitude (h) and time-to-peak (i) of ATP-induced Ca2+ release under conditions shown in (g). j, Cerebellar expression of CLCC1 in the indicated genotypes. GAPDH, loading control. k, ER stress and misfolded protein accumulation documented by Bip and ubiquitin (Ubi) staining, respectively, in cerebella of NM2453 homozygotes (NM/NM) and K298A and NM2453 compound heterozygotes (K298A/NM). P, Purkinje cells. Wildtype (+/+), negative control; NM2453 homozygotes (NM/NM), positive control. l and m, Ubiquitinpositive inclusions in ChAT-positive motor neurons in lumbar 4–5 spinal cords of K298A/NM mice. Representative images (l) and quantification of number of ChAT-positive motor neurons in the ventral horn (m) are shown. n and o, TEM images of cerebellar granule neurons from wildtype (+/+) and K298A/NM mice (n). Red arrows indicate ribosome-bound rough ER. Summary data are shown in (o). Mouse age: j and k, 1.5 month; l and m, +/+, 10 months, K298A/NM, 14 months; n and o, 3 months. Quantification: d, e, and f, n = 4-20; h and i, more than 150 cells from three independent experiments; m and o, 14-18 slides (m) and more than 25 granule cells (o) per mouse from three individual animals for each genotype. Scale bar, k, 20 μm; l, 10 μm; n, 50 nm. Values are presented as mean ± SEM; N.S., no significant difference; *p<0.05; ***p<0.001, by t-test or one-way ANOVA.

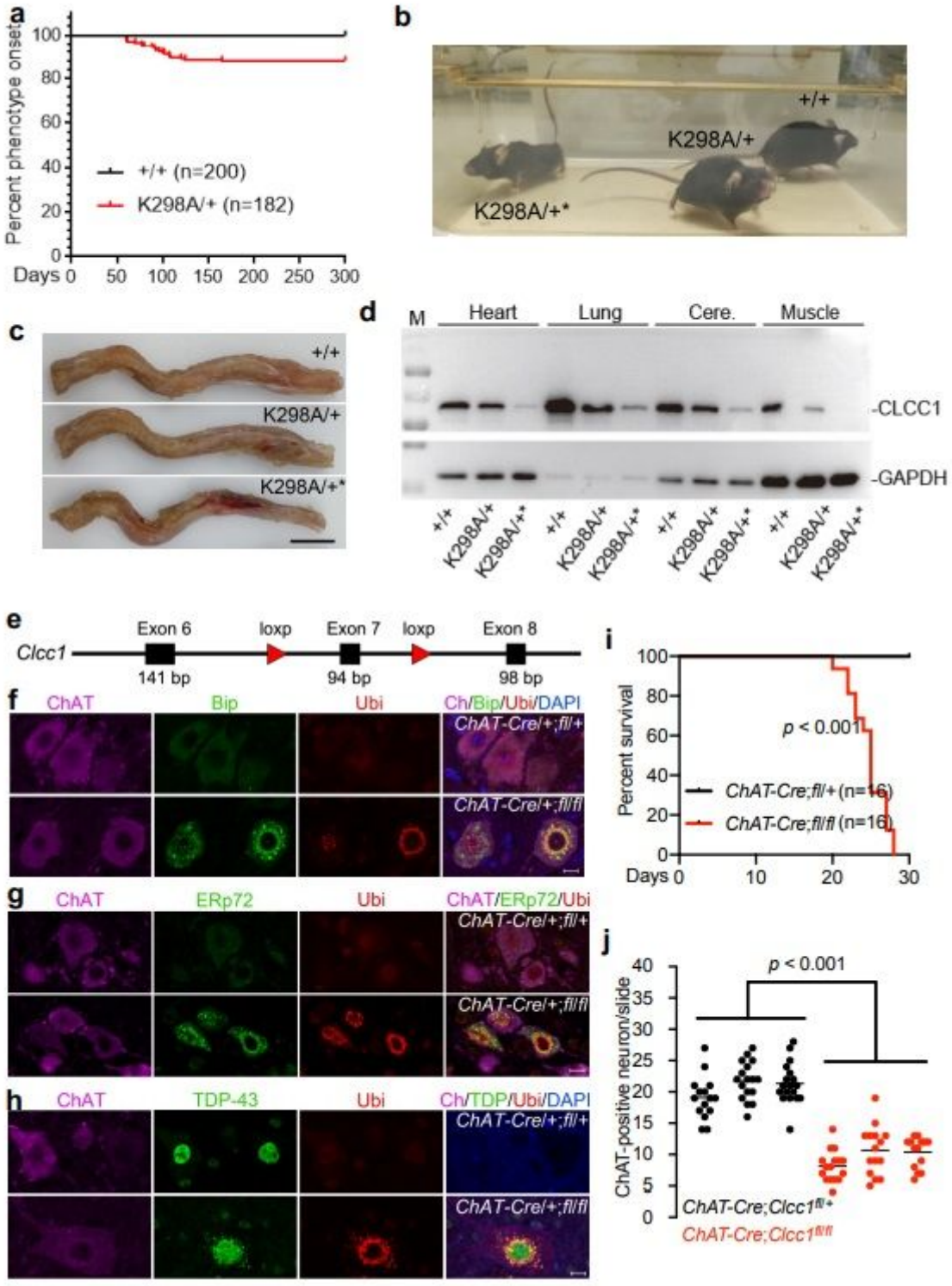

Figure 6

Increased penetrance of K298A allele and cell-autonomous effect of Clcc1 loss-of-function in motor neuron loss. a, Percent of phenotype onset in wildtype (+/+) and K298A/+ animals. The early onset phenotypes of K298A/+ animals (K298A/+*, 12/182, onset time: postnatal 90.9 ± 5.5 days) include body weight loss, hindlimb weakness, trunk shaking, tail flagging, abnormal gaits, and ataxia (also see Movie S2). b, A K298A/+ mutant mouse displaying early onset phenotype (K298A/+*) together with a wildtype

and a normal K298A/+ mouse. c, Curved spine shown in K298A/+* but not in wildtype and K298A/+ mice. d, Expression levels of CLCC1 in various tissues in wildtype, K298A/+, and K298A/+* mice. Summary data in Extended Data Fig. 13. e, Construction of Clcc1 conditional knockout mouse. f-j, Knockout of Clcc1 in ChAT-positive motor neurons (ChAT-Cre;Clcc1fl/fl) leads to ER stress (f and g), TDP-43 pathology (h), early death (i), and motor neuron loss (j). ChAT-Cre;Clcc1fl/+ served as a negative control. In j, 14-18 slides per mouse from lumbar 4–5 spinal cords of three individual animals for each genotype were analyzed. Mouse age: b-d, 10 months; f, g, h, and j, P20-25. Scale bar in f-h, 10 μm.

Supplementary Files

This is a list of supplementary files associated with this preprint. Click to download.

- SupplementaryMovie1LinkCLCC1toALS.mp4
- SupplementaryMovie2LinkCLCC1toALS.mp4
- FiguresLinkCLCC1toALS0516.pdf